

# Superconducting instability in non-Fermi liquids

Ipsita Mandal

*Perimeter Institute for Theoretical Physics, 31 Caroline St. N., Waterloo ON N2L 2Y5, Canada*

We use renormalization group (RG) analysis and dimensional regularization techniques to study potential superconductivity-inducing four-fermion interactions in systems with critical Fermi surfaces of general dimensions ( $m$ ) and co-dimensions ( $d - m$ ), arising as a result of quasiparticle interaction with a gapless Ising-nematic order parameter. These are examples of non-Fermi liquid states in  $d$  spatial dimensions. Our formalism allows us to treat the corresponding zero-temperature low-energy effective theory in a controlled approximation close to the upper critical dimension  $d = d_c(m)$ . The fixed points are identified from the RG flow equations, as functions of  $d$  and  $m$ . We find that the flow towards the non-Fermi liquid fixed point is preempted by Cooper pair formation for both the physical cases of  $(d = 3, m = 2)$  and  $(d = 2, m = 1)$ . In fact, there is a strong enhancement of superconductivity by the order parameter fluctuations at the quantum critical point.

## CONTENTS

I. Introduction	1
II. Ising-nematic quantum critical point	2
III. Superconducting Instability	4
A. One-loop diagrams generating terms proportional to $V_S^2$	5
B. UV-divergent terms proportional to $\tilde{\epsilon}$	5
C. One-loop diagrams generating terms proportional to $\tilde{\epsilon} V_S$	6
D. Beta-functions for the coupling constants	7
E. Fixed points of the beta functions	9
IV. Summary and outlook	10
Acknowledgments	12
A. Computation of the Feynman diagrams proportional to $V_S^2$	12
B. One-loop diagrams proportional to $\tilde{\epsilon} V_S$	13
1. Cancellation of the terms proportional to $\tilde{\epsilon} \tilde{V}_S$ near $m = 2$	15
C. Treatment of the terms proportional to $\tilde{\epsilon}$ in the Wilsonian RG language	16
References	16

## I. INTRODUCTION

Non-Fermi liquids are unconventional metallic states that cannot be studied using the framework of the Landau Fermi liquid theory [1–24]. Such systems can arise when a gapless boson is coupled with a Fermi surface. One class of non-Fermi liquids involve the critical boson carrying zero momentum, such as the Ising-nematic critical point [7, 9, 10, 12, 25–39] and nonrelativistic fermions coupled with an emergent gauge field [40–43]. In another class of non-Fermi liquids, the critical boson carries a non-zero momentum. The examples in this class include the order parameters at the spin density wave (SDW) and charge density wave (CDW) critical points [13–15, 21]. All these non-Fermi liquids have a well-defined Fermi-surface but no well-defined Landau quasiparticles. In other words, although these metallic states do not have a discontinuity in the zero-temperature electron occupation number, the Fermi surface/momentum can be still be sharply defined through the location of weaker non-analyticities of the spectral function [44, 45].

Superconducting instabilities in such non-Fermi liquid scenarios have attracted a lot of attention in the recent literature [46–50]. We addressed this problem for nonrelativistic fermions coupled to a  $U(1)$  gauge field in three spatial dimensions by solving the Dyson-Nambu equation [47]. We used a similar approach to solve for the pairing gap for the cases of the half-filled Landau level state as well the bilayer Hall system with a total filling fraction equal to one [49]. The cases of Ising-nematic critical point, spinon Fermi surface and the Halperin-Lee-Read states involving one-dimensional Fermi surfaces have been discussed in details by Metlitski *et al.* [48] by using renormalization group (RG) techniques and the concept of “inter-patch” couplings.

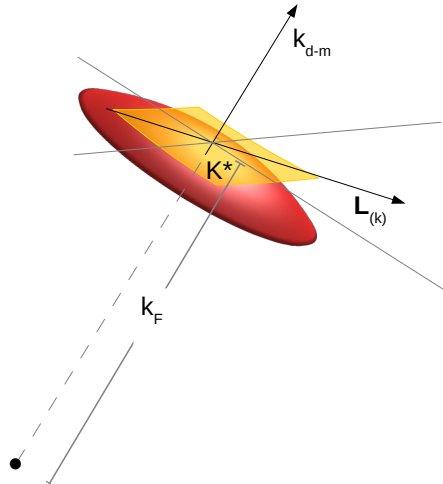


FIG. 1. Cartesian coordinates on a patch of an  $m$ -dimensional convex Fermi surface.

In the present work, we focus on the Ising-nematic quantum critical point involving a Fermi surface of generic dimensions, applying the RG methods developed in our earlier paper [22]. Denoting the dimension of the Fermi surface by  $m$  and the spatial dimensions by  $d$ , the co-dimension is given by  $(d - m)$ . It was shown that there is a non-trivial mixing between the ultraviolet (UV) and infrared (IR) physics for  $m > 1$ , and a perturbative control for such systems can be achieved by tuning both  $m$  and  $(d - m)$  independently. This method also allows one to maintain the locality of the action in real space irrespective of the value of  $m$ , in contrast to the analysis by Metlitski *et al.* [48].

We consider a four-fermion interaction  $V$  in the pairing channel with a tree-level scaling dimension equal to  $-d + 1 + m/2$ . We find that the scatterings in the BCS channel are enhanced by the square root of the Fermi surface volume, which goes as  $k_F^m$ . Consequently, the effective coupling that dictates the potential superconducting instability, is given by  $\tilde{V} = V k_F^{m/2}$ , which has an enhanced scaling dimension of  $-d + 1 + m$ . Clearly,  $\tilde{V}$  is marginal when the co-dimension takes the value  $d - m = 1$ . Our goal is to examine how the interactions of the fermions with critical bosons affect the pairing instability.

The paper is organized as follows: In Sec. II, we review the dimensional regularization procedure devised in our earlier work to obtain a perturbative control of the Ising-nematic quantum critical point. The four-fermion interactions, which can be responsible for potential BCS instability, are introduced in Sec. III. There we compute the divergent terms contributing to the beta-functions to the lowest order. The solutions to the RG equations in various possible scenarios are discussed in Sec. III E. We conclude with a summary and outlook in Sec. IV. The detailed computation of the relevant Feynman diagrams has been shown in the appendix.

## II. ISING-NEMATIC QUANTUM CRITICAL POINT

We consider the Ising-nematic quantum critical point involving an  $m$ -dimensional Fermi surface interacting with a massless boson in  $d = (m + 1)$  space dimensions [22], with coupling constant  $e$ . The momentum of the critical boson is centered at zero. This system can be described by the action

$$\begin{aligned}
 S = & \sum_{s=\pm, j} \int dk \psi_{s,j}^\dagger(k) [i k_0 + s k_1 + \mathbf{L}_{(k)}^2] \psi_{s,j}(k) + \frac{1}{2} \int dk [k_0^2 + k_1^2 + \mathbf{L}_{(k)}^2] \phi(-k) \phi(k) \\
 & + \frac{e}{\sqrt{N}} \sum_{s=\pm, j} \int dk dq \phi(q) \psi_{s,j}^\dagger(k+q) \psi_{s,j}(k), \quad (1)
 \end{aligned}$$

written in a coordinate system centred at an arbitrary point  $K^*$  of the convex Fermi surface (see Fig. 1). Here,  $k$  is the  $(d + 1)$ -dimensional energy-momentum vector with  $dk \equiv \frac{d^{d+1}k}{(2\pi)^{d+1}}$ . Assuming inversion symmetry, we have included the “right-moving” and “left-moving” fermionic fields,  $\psi_{+,j}$  and  $\psi_{-,j}$ , representing  $K^*$  and its antipodal point  $-K^*$ . These fields represent fermions with flavours  $j = 1, 2, \dots, N$ , frequency  $k_0$  and momentum  $K_\alpha^* + k_\alpha$  ( $-K_\alpha^* + k_\alpha$ ) with  $1 \leq \alpha \leq d$ .  $k_1$  and  $\mathbf{L}_{(k)} \equiv (k_2, k_3, \dots, k_d)$  denote the momentum components perpendicular and parallel to the Fermi surface at  $\pm K^*$ ,

respectively. The momenta are rescaled such that the Fermi velocity, and the curvature of the Fermi surface at  $\pm K^*$ , are equal to one.

A perturbative control of the Yukawa coupling (and the strength of UV/IR mixing in non-Fermi liquid states with  $m > 1$  [22]) is achieved by tuning the dimension [51–55] and the co-dimension of the Fermi surface [20, 21, 56], i.e. by writing an action that describes an  $m$ -dimensional Fermi surface embedded in the  $d$ -dimensional momentum space:

$$S = \sum_j \int dk \bar{\Psi}_j(k) \left[ i \boldsymbol{\Gamma} \cdot \mathbf{K} + i \gamma_{d-m} \delta_k \right] \Psi_j(k) \exp \left\{ \frac{\mathbf{L}_{(k)}^2}{\mu \tilde{k}_F} \right\} + \frac{1}{2} \int dk \mathbf{L}_{(k)}^2 \phi(-k) \phi(k) + \frac{i e \mu^{x/2}}{\sqrt{N}} \sum_j \int dk \phi(k) \bar{\Psi}_j(k+q) \gamma_{d-m} \Psi_j(k), \quad (2)$$

where a mass scale  $\mu$  is introduced to make  $\tilde{k}_F$  and  $e$  dimensionless. Here

$$x = -d + 2 + \frac{m}{2}, \quad \delta_k = k_{d-m} + \mathbf{L}_{(k)}^2, \quad k_F = \mu \tilde{k}_F, \quad \Psi_j^T(k) = \left( \psi_{+,j}(k), \psi_{-,j}^\dagger(-k) \right). \quad (3)$$

The gamma matrices associated with  $\mathbf{K}$  have been written as  $\boldsymbol{\Gamma} \equiv (\gamma_0, \gamma_1, \dots, \gamma_{d-m-1})$ . Since in real systems,  $d - m$  lies between 1 and 2, we will consider only the  $2 \times 2$  gamma matrices so that the corresponding spinors always have two components. We will use the representation where

$$\Gamma_0 \equiv \gamma_0 = \sigma_y, \quad \gamma_{d-m} = \sigma_x \quad (4)$$

are fixed in general dimensions. The bare fermion propagator is given by  $G_0(k) = \frac{1}{i} \frac{\boldsymbol{\Gamma} \cdot \mathbf{K} + \gamma_{d-m} \delta_k}{\mathbf{K}^2 + \delta_k^2} \exp \left\{ - \frac{\mathbf{L}_{(k)}^2}{k_F} \right\}$ . Note that we have used an exponential factor in order to damp out the fermion propagator, which acts as a soft cut-off for the directions tangential to the Fermi surface in loop-integrals. This restricts the integration along the directions tangent to the Fermi surface to a small region compared to  $k_F$  by damping the propagation of fermions with  $|\mathbf{L}_{(k)}| > k_F^{1/2}$ . We denote the UV cut-off for  $\mathbf{K}$  and  $k_{d-m}$  as  $\Lambda$ , which is naturally given by the choice  $\Lambda = \mu$ . Hence, two dimensionless parameters,  $e$  and  $\tilde{k}_F = k_F/\Lambda$ , appear in the above action. If  $k$  is the typical energy at which we probe the system, we must impose the restriction  $k \ll \Lambda \ll k_F$ . The renormalization group flow is generated by changing  $\Lambda$  and requiring that low-energy observables are independent of it.

The boson propagator that we will use in our computations includes the one-loop self-energy, and is given by

$$D_1(k) = \frac{1}{\mathbf{L}_{(k)}^2 + \tilde{\alpha} \frac{|\mathbf{K}|^{d-m}}{|\mathbf{L}_{(k)}|}}, \quad \tilde{\alpha} = \beta_d e^2 \mu^x k_F^{\frac{m-1}{2}},$$

$$\beta_d = \frac{\Gamma^2(\frac{d-m+1}{2})}{2^{\frac{2d+m-1}{2}} \pi^{\frac{d-1}{2}} |\cos\{\frac{\pi(d-m+1)}{2}\}| \Gamma(\frac{d-m}{2}) \Gamma(d-m+1)} \quad (5)$$

to the leading order in  $k/k_F$ , for  $|\mathbf{K}|^2/|\mathbf{L}_{(k)}|^2, \delta_k^2/|\mathbf{L}_{(k)}|^2 \ll k_F$ . This is because the bare boson propagator is independent of  $(k_0, \dots, k_{d-m})$ , resulting in the loop integrations involving it being ill-defined. Hence we need to resum a series of diagrams that provides a non-trivial dispersion along these directions [22].

In our previous work [22], it was established that the higher order corrections are controlled not by  $e$ , but by an effective coupling  $\tilde{e}$  with

$$\tilde{e} \equiv \frac{e^{2(m+1)/3}}{\tilde{k}_F^{\frac{(m-1)(2-m)}{6}}}. \quad (6)$$

The form of the one-loop fermion self-energy showed that it blows up logarithmically in  $\Lambda$  at the critical dimension

$$d_c(m) = m + \frac{3}{m+1}. \quad (7)$$

We also found that the RG equations, with the increasing logarithmic length scale  $l = -\ln \mu$ , are given by

$$\frac{\partial \tilde{k}_F}{\partial l} = \tilde{k}_F, \quad \frac{\partial \tilde{e}}{\partial l} = \frac{(m+1)\varepsilon}{3} \tilde{e} - \frac{(m+1)u_1}{3N} \tilde{e}^2, \quad (8)$$

to order  $\tilde{e}^2$ , where  $\varepsilon = d_c - d$  and

$$u_1 = \frac{|\csc\{(m+1)\pi/3\}|}{2^{m-1} \pi^{\frac{m-2}{2}} (4\pi)^{\frac{3}{2(m+1)}} \beta_d^{\frac{2-m}{3}} (m+1)} \frac{\Gamma(\frac{m+4}{2(m+1)})}{\Gamma(m/2) \Gamma(\frac{2-m}{2(m+1)}) \Gamma(\frac{2m+5}{2(m+1)})}. \quad (9)$$

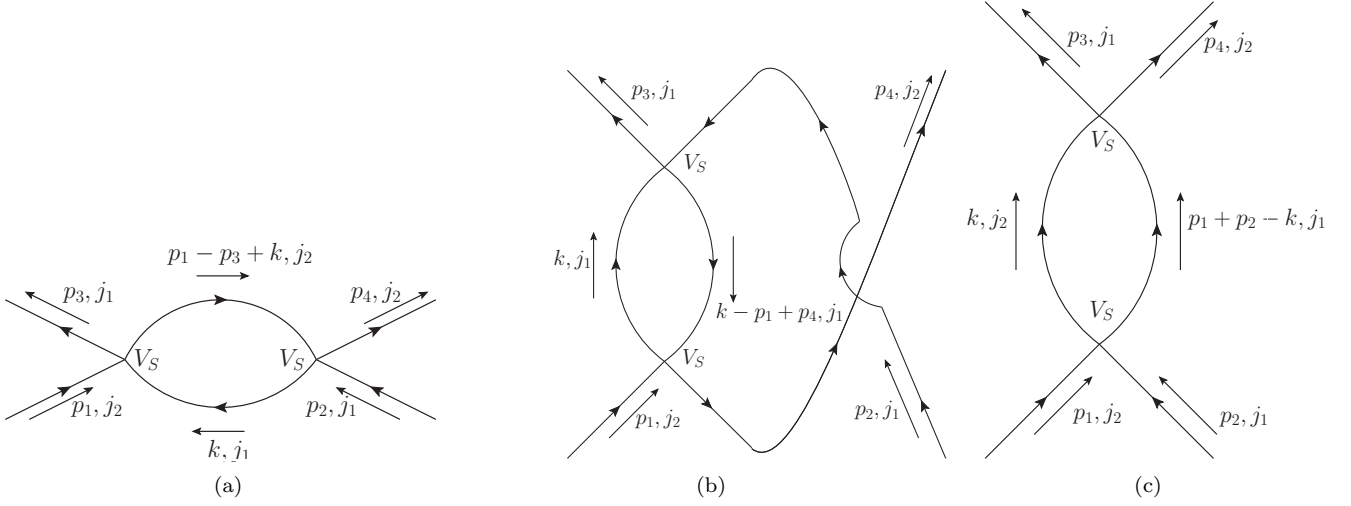


FIG. 2. One-loop diagrams proportional to  $V_S^2$ . Here  $p_4 = p_1 + p_2 - p_3$ .

### III. SUPERCONDUCTING INSTABILITY

With the motivation of analysing superconducting instability for our non-Fermi liquid system, we will add the appropriate four-fermion interaction terms to the action in Eq. (2). We note that:

$$\begin{aligned} & \int \left( \prod_{s=1}^4 dp_s \right) \left[ \{ \bar{\Psi}_{j_1}(p_3) \Psi_{j_2}(p_1) \} \{ \bar{\Psi}_{j_3}(p_4) \Psi_{j_4}(p_2) \} - \{ \bar{\Psi}_{j_3}(p_3) \sigma_z \Psi_{j_4}(p_1) \} \{ \bar{\Psi}_{j_1}(p_4) \sigma_z \Psi_{j_2}(p_2) \} \right] \\ & \quad \times \frac{\mathcal{F}(p_1, p_3; p_2, p_4)}{4} \\ & = - \int \left( \prod_{s=1}^4 dp_s \right) \left[ \psi_{+,j_1}^\dagger(p_3) \psi_{-,j_2}^\dagger(-p_1) \psi_{-,j_3}(-p_4) \psi_{+,j_4}(p_2) \right] \mathcal{F}(p_1, p_3; p_2, p_4), \end{aligned}$$

can give rise to BCS pairing, where  $\mathcal{F}(p_1, p_3; p_2, p_4)$  is a function invariant under the simultaneous exchanges  $(p_1, p_3) \leftrightarrow (p_2, p_4)$ . Hence, we need to consider the four-fermion terms:

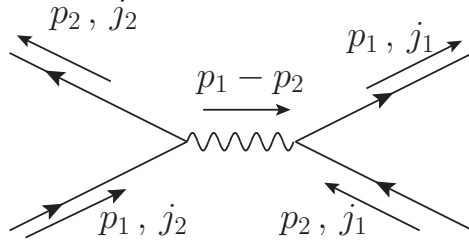
$$\begin{aligned} S_{\text{gen}}^{\text{SC}} &= \frac{\mu^{d_v}}{4} \sum_{j_1, j_2, j_3, j_4} \int \left( \prod_{s=1}^4 dp_s \right) (2\pi)^{d+1} \delta^{(d+1)}(p_1 + p_2 - p_3 - p_4) \\ & \quad \times \left[ \{ \bar{\Psi}_{j_1}(p_3) \Psi_{j_2}(p_1) \} \{ \bar{\Psi}_{j_3}(p_4) \Psi_{j_4}(p_2) \} - \{ \bar{\Psi}_{j_3}(p_3) \sigma_z \Psi_{j_4}(p_1) \} \{ \bar{\Psi}_{j_1}(p_4) \sigma_z \Psi_{j_2}(p_2) \} \right], \\ & \quad \times \left[ V_S(\mathbf{p}_1, \mathbf{p}_3; \mathbf{p}_2, \mathbf{p}_4) (\delta_{j_1, j_3} \delta_{j_2, j_4} - \delta_{j_1, j_4} \delta_{j_2, j_3}) + V_A(\mathbf{p}_1, \mathbf{p}_3; \mathbf{p}_2, \mathbf{p}_4) (\delta_{j_1, j_3} \delta_{j_2, j_4} + \delta_{j_1, j_4} \delta_{j_2, j_3}) \right] \end{aligned} \quad (10)$$

where  $\mathbf{k}$  denotes the momentum components,  $(k_{d-m}, \mathbf{L}_{(k)})$ , of the  $(d+1)$ -dimensional energy-momentum vector  $k$ . The subscript ‘‘S’’ (‘‘A’’) denotes that  $V_S(\mathbf{p}_1, \mathbf{p}_3; \mathbf{p}_2, \mathbf{p}_4)$  ( $V_A(\mathbf{p}_1, \mathbf{p}_3; \mathbf{p}_2, \mathbf{p}_4)$ ) is symmetric (antisymmetric) under the interchange  $p_1 \leftrightarrow p_3$  or  $p_2 \leftrightarrow p_4$ . Here we have made the  $V_{S/A}$ ’s dimensionless by using the mass scale  $\mu$ , with  $d_v = -d + 1 + \frac{m}{2}$  representing the scaling dimension of  $V_{S/A}$ .

We will find from our analysis of the RG flow, in order for superconducting instability to set in, we must have  $\mathbf{p}_1 = \mathbf{p}_3$  and  $\mathbf{p}_2 = \mathbf{p}_4$ . Furthermore, assumption of rotational symmetry allows us to write:

$$V_{S/A}(\mathbf{p}_1, \mathbf{p}_1; \mathbf{p}_2, \mathbf{p}_2) = V_{S/A}(\theta_1 - \theta_2), \quad (11)$$

where  $\theta_{1,2}$  denote the angles for  $\mathbf{p}_{1,2}$  on the Fermi surface. For simplicity and in order to obtain analytic expressions, we will consider only the case of a constant non-zero  $V_S$ , for which we need at least two flavours of fermions. Then, with

FIG. 3. Tree-level diagram proportional to  $e^2$ .

$N = 2$ , Eq. (10) reduces to:

$$S^{\text{sc}} = -\frac{\mu^{d_v} V_S}{4} \sum_{j_1, j_2} \int \left( \prod_{s=1}^4 dp_s \right) (2\pi)^{d+1} \delta^{(d+1)}(p_1 + p_2 - p_3 - p_4) (1 - \delta_{j_1, j_2}) \\ \times \left[ \{ \bar{\Psi}_{j_1}(p_3) \Psi_{j_2}(p_1) \} \{ \bar{\Psi}_{j_2}(p_4) \Psi_{j_1}(p_2) \} - \{ \bar{\Psi}_{j_1}(p_3) \sigma_z \Psi_{j_2}(p_1) \} \{ \bar{\Psi}_{j_2}(p_4) \sigma_z \Psi_{j_2}(p_1) \} \right], \quad (12)$$

It is straightforward to apply our formalism for a system with a given number of flavours and a specific angular dependence of  $V_{S/A}$ .

### A. One-loop diagrams generating terms proportional to $V_S^2$

We need to consider one-loop diagrams as shown in Fig. 2 for contributions proportional to  $V_S^2$ . The computation of these diagrams has been detailed in Appendix A. The contribution from Fig. 2a is found to be proportional to:

$$-(1 - \delta_{j_1, j_2})^2 \int dk \text{Tr} [G_0(k + \mathbf{P}_1 - \mathbf{P}_3) G_0(k)] = \frac{2^{1-2d+\frac{m}{2}} (1 - \delta_{j_1, j_2}) k_F^{m/2} \pi^{1-\frac{d}{2}} \sec\left(\frac{(d-m)\pi}{2}\right)}{\Gamma\left(\frac{d-m}{2}\right) |\mathbf{P}_3 - \mathbf{P}_1|^{-d+m+1}}, \quad (13)$$

which is logarithmically divergent at  $d-m=1$  such that we can express it as  $\frac{k_F^{m/2} \ln\left(\frac{|\mathbf{P}_1 - \mathbf{P}_3|}{\Lambda}\right)}{2^{\frac{3m}{2}} \pi^{1+\frac{m}{2}}}$ . The results from Figs. 2b and 2c are  $k_F$ -suppressed and hence do not contribute to the beta-functions.

Noting that  $\text{Tr}[\sigma_z G_0(k + \mathbf{P}_1 - \mathbf{P}_3) \sigma_z G_0(k)] = -\text{Tr}[G_0(k + \mathbf{P}_1 - \mathbf{P}_3) G_0(k)]$ , the full contribution from all one-loop diagrams proportional to  $V_S^2$  is given by:

$$t_{VV} = \frac{4 \times 2}{2!} \frac{4}{4 \times 4} \times \frac{2^{2+2d-\frac{m}{2}} k_F^{m/2} \mu^{2d_v} V_S^2}{\pi^{\frac{d}{2}} \Gamma\left(\frac{d-m}{2}\right) \epsilon} + \mathcal{O}(\epsilon) = \frac{v_2 \mu^{2d_v+\frac{m}{2}} \tilde{k}_F^{m/2} V_S^2}{\epsilon} + \mathcal{O}(\epsilon), \\ v_2 = \frac{2^{2-2d+\frac{m}{2}}}{\pi^{\frac{d}{2}} \Gamma\left(\frac{d-m}{2}\right)}, \quad (14)$$

for  $d-m=1-\epsilon$ .

### B. UV-divergent terms proportional to $\tilde{\epsilon}$

Following earlier studies [46, 48], we have to include contributions from tree-level BCS channel, which are generated from long-range interactions between the fermions. In this case, the long-range interaction is mediated by the massless boson. Here we treat this contribution in the language of dimensional regularization as we have done for the other terms. In Appendix C, we have provided an alternative treatment of these terms in the more familiar Wilsonian RG language.

We consider Fig. 3, which gives the terms

$$\sum_{j_1, j_2} \left[ -\psi_{+,j_1}^\dagger(p_2) \psi_{-,j_2}^\dagger(-p_2) \psi_{-,j_2}(-p_1) \psi_{+,j_1}(p_1) - \psi_{+,j_1}^\dagger(p_1) \psi_{-,j_2}^\dagger(-p_1) \psi_{-,j_2}(-p_2) \psi_{+,j_1}(p_2) \right. \\ \left. - \psi_{+,j_1}^\dagger(p_2) \psi_{+,j_1}(p_1) \psi_{+,j_2}^\dagger(p_1) \psi_{+,j_2}(p_2) - \psi_{-,j_2}^\dagger(-p_2) \psi_{-,j_2}(-p_1) \psi_{-,j_1}^\dagger(-p_1) \psi_{-,j_1}(-p_2) \right]$$

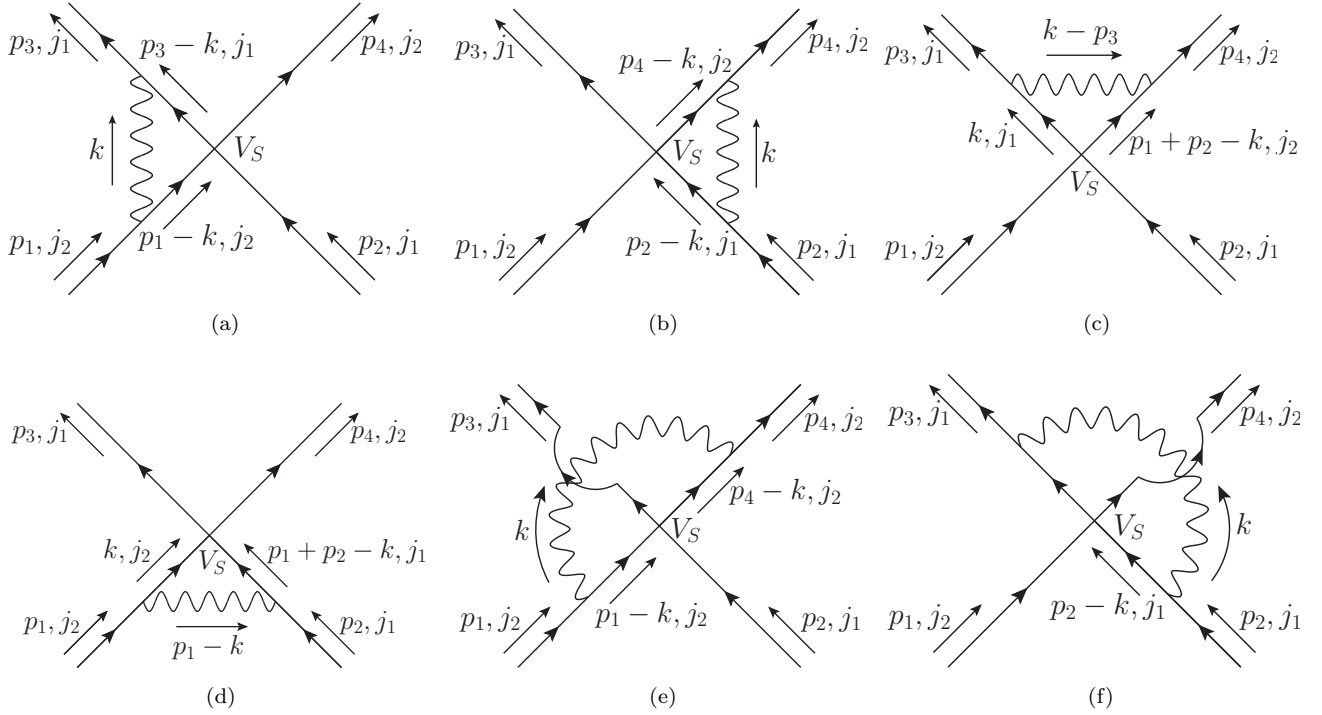


FIG. 4. One-loop diagrams proportional to  $\tilde{e}V_S$ , each consisting of two fermionic and one bosonic propagators forming the loop. Here  $p_4 = p_1 + p_2 - p_3$ ,  $\mathbf{p}_1 = \mathbf{p}_3$  and  $\mathbf{p}_2 = \mathbf{p}_4$ .

multiplying  $\frac{(ie)^2 \mu^x D_1(p_1 - p_2)}{2N}$ . Due to symmetry of  $D_1(p_1 - p_2)$  under  $p_1 \leftrightarrow p_2$ , they contribute as  $\frac{e^2 \mu^x D_1(p_1 - p_2)}{N}$  for terms responsible for BCS instability.

Using  $\mathbf{L}_{(q)}^2 \simeq 2k_F^2(1 - \cos\theta)/k_F \Rightarrow |\mathbf{L}_{(q)}| \simeq \sqrt{k_F}|\theta|$ , the decomposition into angular momentum channels for an  $m$ -dimensional Fermi surface leads to the contribution being proportional to:

$$\begin{aligned}
 t_{ee} &\simeq \frac{e^2 \Lambda^x}{2N} \times 2 \int_{\theta>0} d\theta \frac{\theta^{m-1} |\mathbf{L}_{(q)}|}{\mathbf{L}_{(q)}^3 + \tilde{\alpha} |\mathbf{Q}|^{d-m}} = \frac{e^2 \Lambda^x}{N k_F^{m/2}} \int_{\theta>0} d|\mathbf{L}_{(q)}| \frac{|\mathbf{L}_{(q)}|^m}{\mathbf{L}_{(q)}^3 + \tilde{\alpha} |\mathbf{Q}|^{d-m}} \\
 &= \frac{e^2 \Lambda^x \Gamma(\frac{m+1}{3}) \Gamma(\frac{2-m}{3})}{3 N k_F^{m/2} \tilde{\alpha}^{\frac{2-m}{3}} |\mathbf{Q}|^{\frac{(d-m)(2-m)}{3}}}, \tag{15}
 \end{aligned}$$

which is independent of the angular momentum channel. This expression tells us that for  $m = 2 - \delta$  and  $d = m + 1 - \gamma\varepsilon$ , we get a pole such that  $t_{ee} \simeq \frac{\tilde{e} \Lambda^{\gamma\varepsilon + \frac{(2-m)(m-1)}{6}} \Gamma(\frac{m+1}{3})}{\beta_d^{\frac{2-m}{3}} N k_F^{m/2}} \frac{1}{\delta}$ , which is equivalent to the logarithmically divergent term  $\frac{e^2 \Lambda^x \Gamma(\frac{m+1}{3})}{N k_F^{m/2}} \ln\left(\frac{\sqrt{k_F}}{\tilde{\alpha}^{\frac{1}{3}} |\mathbf{Q}|^{\frac{d-m}{3}}}\right)$ . This term, when continued to the strongly coupled regime of  $m = 1$ , will translate into the infrared divergence there. The resulting counterterm is given by

$$\begin{aligned}
 &-\frac{\mu^{\lambda_1 \varepsilon} \tilde{e} v_1}{4 N a \varepsilon} \sum_{j_1, j_2} \int \left( \prod_{s=1}^4 dp_s \right) (2\pi)^{d+1} \delta^{(d+1)}(p_1 + p_2 - p_3 - p_4) (1 - \delta_{j_1, j_2}) \\
 &\quad \times \left[ \{\bar{\Psi}_{j_1}(p_3) \Psi_{j_2}(p_1)\} \{\bar{\Psi}_{j_1}(p_4) \Psi_{j_2}(p_2)\} - \{\bar{\Psi}_{j_1}(p_3) \sigma_z \Psi_{j_2}(p_1)\} \{\bar{\Psi}_{j_1}(p_4) \sigma_z \Psi_{j_2}(p_2)\} \right], \\
 \lambda_1 &= 1 - \frac{a(7 - m^2)}{6(m+1)}, \quad a\varepsilon = 2 - m, \quad v_1 = \frac{\Gamma(\frac{m+1}{3})}{\beta_d^{\frac{2-m}{3}}}. \tag{16}
 \end{aligned}$$

### C. One-loop diagrams generating terms proportional to $\tilde{e}V_S$

The set of one-loop diagrams which can generate terms proportional to  $\tilde{e}V_S$  are shown in Fig. 4. The computation of these diagrams has been detailed in Appendix B. There it has been found that only Figs. 4a and 4b contribute. After cancellation with the appropriate diagrams in Fig. 5 consisting of counterterm vertices, as explained in Appendix B1,

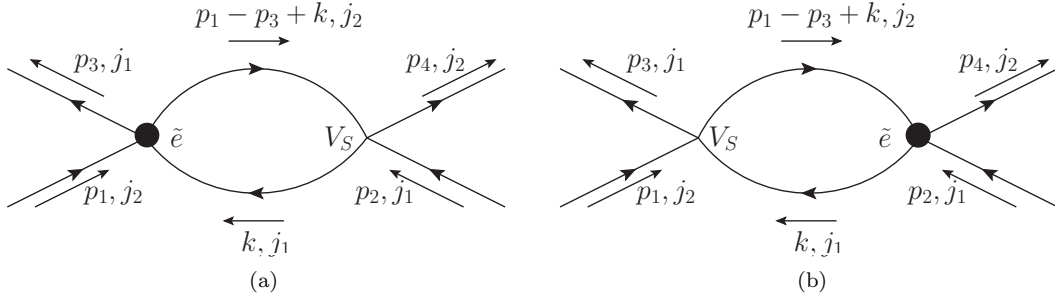


FIG. 5. One-loop diagrams proportional to  $\tilde{e} V_S$ , resulting from counterterms. The counterterm vertex has been denoted by a blob. Here  $p_4 = p_1 + p_2 - p_3$ .

their contribution to the beta-function is captured by the term

$$\left(\frac{v_3}{a} + v_4\right) \frac{\tilde{e} V_S \mu^{(\lambda_2 + \gamma)\epsilon}}{N \epsilon}, \quad (17)$$

where

$$v_3 = \frac{2\gamma_E}{\beta_d^{\frac{2-m}{3}} (2\pi)^{\frac{3}{5-m} + m - 2} \Gamma\left(\frac{m}{2}\right) \Gamma\left(\frac{3}{2(m+1)}\right) \pi}, \quad v_4 = \frac{3v_3}{m+1} - \frac{2}{3}, \quad \lambda_2 = \frac{a(m-1)}{6}. \quad (18)$$

Furthermore, the contribution from Figs. 5a and 5b, after cancellation with Figs. 4a and 4b, is given by:

$$\left(\frac{v_5}{\gamma} + \frac{v_6}{a}\right) \frac{\tilde{e} V_S \mu^{\lambda_1 \epsilon}}{N \epsilon}, \quad (19)$$

where

$$v_5 = -\frac{2^{5-2d+\frac{m}{2}} \gamma_E \Gamma\left(\frac{m+1}{3}\right)}{\beta_d^{\frac{2-m}{3}} \pi^{\frac{d}{2}} \Gamma\left(\frac{d-m}{2}\right)}, \quad v_6 = -v_5. \quad (20)$$

There are two more diagrams in this class, as shown in Fig. 6. Due to the vanishing of the trace of the gamma matrices in the fermionic loop, they are identically zero.

#### D. Beta-functions for the coupling constants

We have found that the one-loop divergent terms are proportional to  $\frac{k_F^{\frac{m}{2}} \mu^{2d_v}}{\gamma \epsilon} V_S^2$  for  $d-m = 1 - \gamma \epsilon$ , for  $|\gamma \epsilon| \ll 1$ . Hence, the upper critical dimension for the four-fermion BCS interaction is  $\tilde{d}_c = m + 1$ , which is different from  $d_c = m + \frac{3}{m+1}$  for the Yukawa coupling (see Eq. (7)). For  $m = 2$ ,  $d_c = \tilde{d}_c = 3$ . However, for  $m = 1$ ,  $d_c = 5/2$  and  $\tilde{d}_c = 2$ . In order to study both the physically relevant cases of  $m = 1$  and  $m = 2$ , we define  $\gamma$  and  $\epsilon$  such that

$$d_c - \epsilon = \tilde{d}_c - \gamma \epsilon \quad \Rightarrow \quad \gamma \epsilon = \epsilon - \frac{2-m}{m+1}. \quad (21)$$

Furthermore, from the form of the divergent terms, it is apparent that

$$\tilde{V}_S = \tilde{k}_F^{m/2} V_S \quad (22)$$

is the effective coupling constant for the four-fermion interactions, which has an enhanced tree-level scaling dimension given by  $d_v + 1/2 = \tilde{d}_c - d$ .  $\tilde{V}_S$  is marginal when the co-dimension  $d - m = 1$ .

The counterterms for the four-fermion interaction term take the form:

$$S_{ct}^{sc} = -\frac{\mu^{\gamma \epsilon} \tilde{A}_S \tilde{V}_S}{4} \sum_{j_1, j_2} \int \left( \prod_{s=1}^4 dp_s \right) (2\pi)^{d+1} \delta^{(d+1)}(p_1 + p_2 - p_3 - p_4) (1 - \delta_{j_1, j_2}) \\ \times \left[ \{ \bar{\Psi}_{j_1}(p_3) \Psi_{j_2}(p_1) \} \{ \bar{\Psi}_{j_1}(p_4) \Psi_{j_2}(p_2) \} - \{ \bar{\Psi}_{j_1}(p_3) \sigma_z \Psi_{j_2}(p_1) \} \{ \bar{\Psi}_{j_1}(p_4) \sigma_z \Psi_{j_2}(p_2) \} \right], \quad (23)$$

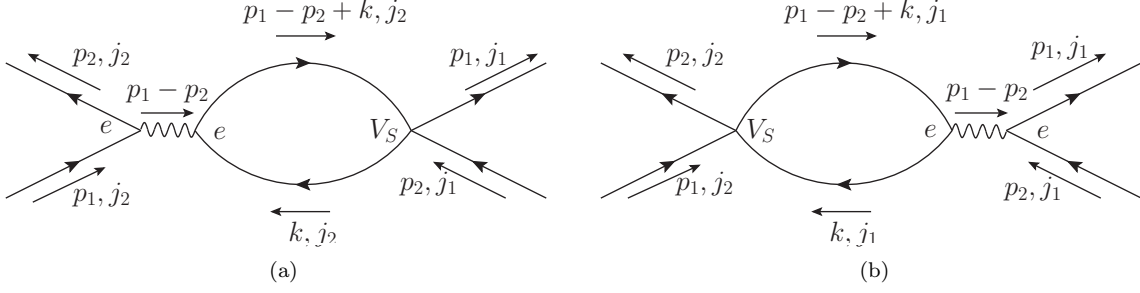


FIG. 6. One-loop diagrams proportional to  $e^2 V_S$ , each consisting of two Yukawa vertices and one fermionic loop.

where we use the definition

$$\tilde{A}_S \equiv \tilde{Z}_S - 1 = \sum_{\alpha_1=1}^{\infty} \frac{\tilde{Z}_{S,\alpha_1}(\tilde{e}, \tilde{k}_F, V_S)}{\varepsilon^{\alpha_1}}. \quad (24)$$

Adding the counterterms to the original  $S^{\text{SC}}$ , and denoting the bare quantities by the superscript “B”, we obtain the renormalized four-fermion interaction as:

$$\begin{aligned} S_{\text{ren}}^{\text{SC}} = & -\frac{V_S^{\text{B}}}{4} \sum_{j_1, j_2} \int \left( \prod_{s=1}^4 dp_s^{\text{B}} \right) (2\pi)^{d+1} \delta^{(d+1)}(p_1^{\text{B}} + p_2^{\text{B}} - p_3^{\text{B}} - p_4^{\text{B}}) (1 - \delta_{j_1, j_2}) \\ & \times \left[ \{ \bar{\Psi}_{j_1}^{\text{B}}(p_3) \Psi_{j_2}^{\text{B}}(p_1) \} \{ \bar{\Psi}_{j_1}^{\text{B}}(p_4) \Psi_{j_2}^{\text{B}}(p_2) \} - \{ \bar{\Psi}_{j_1}^{\text{B}}(p_3) \sigma_z \Psi_{j_2}^{\text{B}}(p_1) \} \{ \bar{\Psi}_{j_1}^{\text{B}}(p_4) \sigma_z \Psi_{j_2}^{\text{B}}(p_2) \} \right], \end{aligned} \quad (25)$$

where

$$\begin{aligned} \mathbf{K} &= \frac{Z_2}{Z_1} \mathbf{K}_B, \quad k_{d-m} = k_{B,d-m}, \quad \mathbf{L}_{(k)} = \mathbf{L}_{(k),B}, \quad \Psi(k) = Z_{\Psi}^{-1/2} \Psi_B(k_B), \quad \phi(k) = Z_{\phi}^{-1/2} \phi_B(k_B), \\ e_B &= Z_3^{-1/2} \left( \frac{Z_2}{Z_1} \right)^{(d-m)/2} \mu^{x/2} e, \quad k_F = \mu \tilde{k}_F, \quad V_S^{\text{B}} k_F^{m/2} = \tilde{Z}_S Z_{\psi}^{-2} \left( \frac{Z_2}{Z_1} \right)^{3(d-m)} \mu^{\gamma \varepsilon} \tilde{V}_S. \end{aligned} \quad (26)$$

The dynamical critical exponent and the anomalous dimension for the fermions are given by [22]:

$$z = 1 + \frac{m+1}{3N} u_1 \tilde{e}, \quad \eta_{\psi} = (1-z)(d-m)/2, \quad (27)$$

with  $u_1$  defined in Eq. (9). Using the definition  $2-m = a\varepsilon \Rightarrow a = \frac{3(1-\gamma)}{1+(1-\gamma)\varepsilon}$ , we have

$$\frac{\tilde{Z}_{S,1} \tilde{V}_S \mu^{\gamma \varepsilon}}{\varepsilon} = \frac{\left( \frac{v_1}{a} + \frac{v_5 \tilde{V}_S}{\gamma} + \frac{v_6 \tilde{V}_S}{a} \right) \tilde{e} \mu^{\lambda_1 \varepsilon}}{N \varepsilon} + \frac{v_2 \tilde{V}_S^2 \mu^{\gamma \varepsilon}}{\gamma \varepsilon} + \frac{\left( \frac{v_3}{a} + v_4 \right) \tilde{e} \tilde{V}_S \mu^{(\lambda_2 + \gamma) \varepsilon}}{N \varepsilon}. \quad (28)$$

Implementing the condition  $\frac{d}{d \ln \mu} \left( V_S^{\text{B}} k_F^{m/2} \right) = 0$ , we get

$$\begin{aligned} \beta_V + \frac{\left\{ \frac{v_1}{a} + \left( \frac{v_3+v_6}{a} + v_4 + \frac{v_5}{\gamma} \right) \tilde{V}_S \right\} \tilde{\beta}_e + \left( \frac{v_3+v_6}{a} + v_4 + \frac{v_5}{\gamma} \right) \beta_V \tilde{e}}{N \varepsilon} + \frac{2v_2 \tilde{V}_S \beta_V}{\gamma \varepsilon} + \{ \gamma \varepsilon - 4\eta_{\psi} + 3(d-m)(1-z) \} \left( \tilde{V}_S + \frac{v_2 \tilde{V}_S^2}{\gamma \varepsilon} \right) \\ + \{ \lambda_1 \varepsilon - 4\eta_{\psi} + 3(d-m)(1-z) \} \frac{\left( \frac{v_1}{a} + \frac{v_5 \tilde{V}_S}{\gamma} + \frac{v_6 \tilde{V}_S}{a} \right) \tilde{e}}{N \varepsilon} + \{ (\lambda_2 + \gamma) \varepsilon - 4\eta_{\psi} + 3(d-m)(1-z) \} \frac{\left( \frac{v_3}{a} + v_4 \right) \tilde{e} \tilde{V}_S}{N \varepsilon} = 0, \end{aligned} \quad (29)$$

where  $\beta_V \equiv \frac{\partial \tilde{V}_S}{\partial \ln \mu} = \beta_V^{(0)} + \beta_V^{(1)} \varepsilon$ ,  $\tilde{\beta}_e \equiv \frac{\partial \tilde{e}}{\partial \ln \mu} = -\frac{m+1}{3} \varepsilon \tilde{e} + \mathcal{O}(\tilde{e}^2)$ .

Comparing the coefficients of the different powers of  $\varepsilon$  on both sides, the solution takes the form:

$$\frac{\partial \tilde{V}_S}{\partial l} = \gamma \varepsilon \tilde{V}_S - v_2 \tilde{V}_S^2 - \frac{(7-m^2)v_1}{6N(m+1)} \tilde{e} + \left[ \frac{(5-m^2-2m)(3v_5-v_6)}{m+1} + (m-1)v_3 - 2(m+1)(u_1+v_4) \right] \frac{\tilde{e} \tilde{V}_S}{6N}, \quad (30)$$

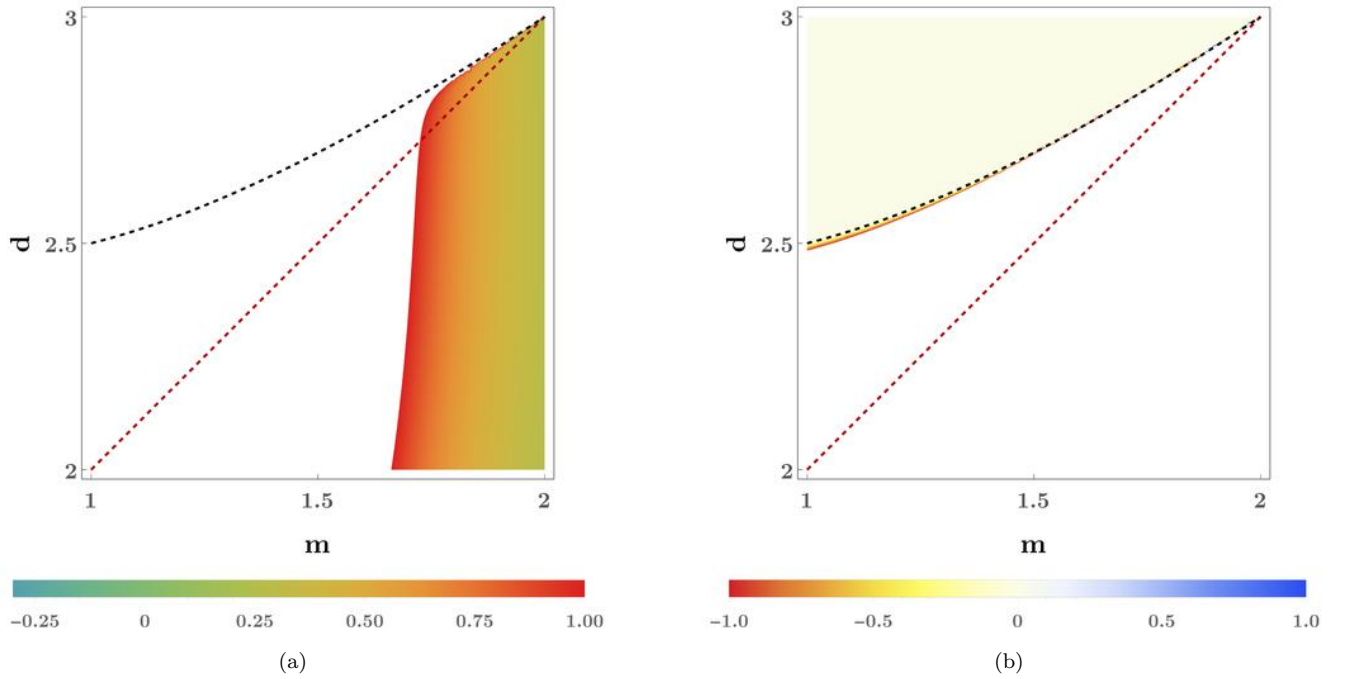


FIG. 7. The contourplots of the two fixed points ( $\tilde{V}_S^*$ ) of  $\beta_V$  as functions of  $d$  and  $m$ . The intersection of the white areas in the two density-plots corresponds to regions where no perturbative fixed point exists. The dashed black(red) curve(line) represents  $d = d_c$  ( $d = \tilde{d}_c$ ) in each plot.

upto  $\mathcal{O}(\tilde{\varepsilon}^2, \tilde{\varepsilon}\varepsilon, \varepsilon^2)$  in one-loop corrections. This can be simplified as:

$$\frac{\partial \tilde{V}_S}{\partial l} = \begin{cases} (\varepsilon - \frac{1}{2}) \tilde{V}_S - v_2 \tilde{V}_S^2 - \frac{v_1}{2N} \tilde{\varepsilon} + \frac{3v_5 - 4v_4 - v_6 - 4u_1}{6N} \tilde{\varepsilon} \tilde{V}_S & \text{for } m = 1, \\ \gamma \varepsilon \tilde{V}_S - v_2 \tilde{V}_S^2 - \frac{v_1}{6N} \tilde{\varepsilon} + \frac{v_3 + 6v_4 - 3v_5 + v_6 - 6u_1}{6N} \tilde{\varepsilon} \tilde{V}_S & \text{for } m = 2 \text{ and } \gamma = \pm 1. \end{cases} \quad (31)$$

The RG flows for some representative values of  $(d, m)$  have been plotted in Fig. 9.

### E. Fixed points of the beta functions

The fixed points for the beta functions can be found from the solutions of  $\frac{\partial \tilde{V}_S}{\partial l} = 0$  and  $\frac{\partial \tilde{\varepsilon}}{\partial l} = 0$ , using Eqs. (8) and (31). The quadratic equation for the fixed point values of  $\tilde{V}_S = \tilde{V}_S^*$  gives two roots. The contourplots of the values of these two roots as functions of  $m$  and  $d$  have been shown in Figs. 7 and 8, restricting to the range  $|\tilde{V}_S^*| < 1$ . The reason for the restriction is that we must be careful not to go outside the window where the perturbation theory makes sense. The intersection of the white areas in the two subfigures of Fig. 7 corresponds to regions where no perturbative solution exists and the system is eventually driven to superconducting state where  $\tilde{V}_S^*$  enters the strong coupling regime with large negative values (i.e., no longer within the perturbative regime), irrespective of the initial value of  $\tilde{V}_S$  from which we start the RG flow. RG flows for some representative values of  $m$  and  $d$  have been plotted in Fig. 9 in order to understand the stability of the fixed points. We observe the following:

1. At  $(d = 3, m = 2)$ , there is only finite solution given by  $(\tilde{V}_S^* = 0, \tilde{\varepsilon}^* = 0)$ , corresponding to an IR unstable fixed point [cf. Fig. 9d]. This implies that for an initial  $\tilde{\varepsilon} = 0$ , the system becomes superconducting only when the initial  $\tilde{V}_S$  is negative, corresponding to the usual BCS instability in the Fermi liquid scenario. However, starting with any value of  $\tilde{\varepsilon} > 0$  drives the system to the strong-coupling regime with large negative  $\tilde{V}_S$ , irrespective of the initial value of  $\tilde{V}_S$ . In other words, the system is unstable to superconductivity even for positive initial values of  $\tilde{V}_S$ , in contrast with the case of Fermi liquids.<sup>1</sup> Hence, in this region, the non-Fermi liquid is unstable to superconducting instability with an enhancement brought about by the order parameter fluctuations.

<sup>1</sup> We would like to emphasize that the  $(d = 3, m = 2)$  Fermi liquids are also unstable to Cooper pairing for an infinitesimally weak interaction regardless of its sign, but in some higher angular momentum channel ( $\ell > 0$ ) [57]. For the Ising-nematic case under study, such an instability occurs for all angular momentum channels.

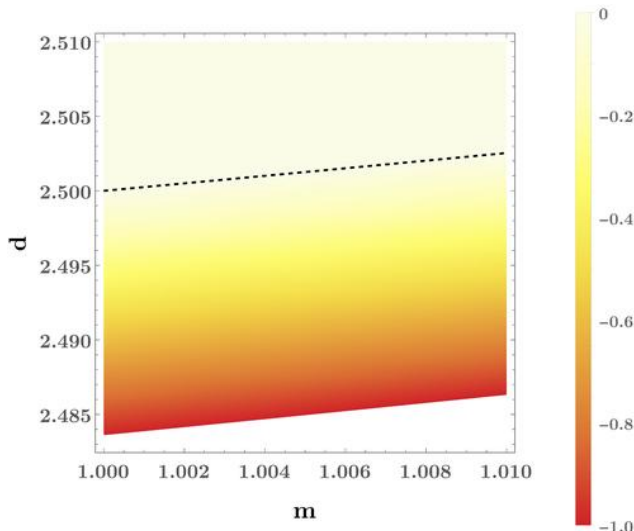


FIG. 8. The contourplot of the second root obtained from  $\beta_V = 0$ , representing a fixed point value  $\tilde{V}_S^*$ , as a function of  $m$  and  $d$ . Here we have enlarged the region around  $m = 1$ . The dashed black line represents  $d = d_c$ .

- Let us first focus on the region near  $(d = 5/2, m = 1)$ , which has been magnified in Fig. 8. In a very thin slice below  $d_c$  for  $m = 1$ , we find that there are two perturbative solutions, namely  $(\tilde{V}_S^* = -f_1, \tilde{e}^* = \frac{N\varepsilon}{u_1})$  and  $(\tilde{V}_S^* = 0, \tilde{e}^* = 0)$ , where  $0 < f_1 < 1$  (e.g., Fig. 9a). In this region, the non-Fermi liquid is stable for a given initial  $\tilde{e} > 0$ . However, if we switch our focus to the wide regions around region  $(d = 2, m = 1)$ , no perturbative solution for  $\tilde{V}_S^*$  exists and the system is unstable to superconductivity even for repulsive initial values of  $\tilde{V}_S$  (e.g., Fig. 9c). This is applicable for  $m = 1$  and  $d = d_c - \varepsilon$ , with  $\varepsilon \gtrsim 0.017$ . The Ising-nematic order parameter fluctuations thus lead to strong enhancement of superconducting instability in the physical region of interest, which is the region around  $(d = 2, m = 1)$ . But, unfortunately, our calculations are not perturbatively controlled in this region, as  $\tilde{e}$  is not infinitesimally small for  $\varepsilon \sim 1/2$ , and we have derived our RG equations assuming that we are looking for poles in  $1/\varepsilon$ . Nevertheless, if we assume that we can continuously extrapolate to the physical case of  $\varepsilon = 1/2$ , we conclude that the pairing instability is strongly enhanced near the  $(2 + 1)$ -d Ising-nematic critical point and the destruction of quasiparticles is preempted by Cooper pairing, in agreement with Ref. [48].

A few comments are in order regarding the enhanced superconductivity near  $(d = 3, m = 2)$  and  $(d = 2, m = 1)$ . The Yukawa-like coupling  $\tilde{e}$  gives rise to an effective attractive interaction for Cooper pairing and hence drives the system towards superconductivity even with an initially positive value of  $\tilde{V}_S$ , as long as  $\tilde{e}$  is non-zero, as the flow continues towards  $\tilde{V}_S^*$  with large negative values. It can be shown that the energy scale at which this happens is always larger than the non-Fermi liquid energy scale (i.e., the scale where the non-Fermi liquid effects become appreciable). However, the magnitude of the pairing gap will depend on the initial values of the coupling constants. An analysis along these lines is very similar to that of Metlitski *et al.* [48] and their estimate regarding the pairing gap holds after taking appropriate values of  $\varepsilon$ , namely  $\varepsilon \simeq 0$  and  $\varepsilon = 1/2$  for solving the  $(d = 3, m = 2)$  and  $(d = 2, m = 1)$  cases respectively.

#### IV. SUMMARY AND OUTLOOK

We have used RG to study potential superconducting instability induced by four-fermion interactions for Ising-nematic quantum critical points, in a perturbative expansion near the upper critical dimension  $d_c(m)$  of the order parameter coupling with quasiparticles. Using the small parameter  $\varepsilon = d_c(m) - d$ , the RG flow equations and fixed points for both the effective order parameter coupling  $\tilde{e}$  and BCS-channel coupling  $\tilde{V}_S$  have been computed as functions of  $d$  and  $m$ . We have found that for  $(d = 3, m = 2)$ , the flow towards the non-Fermi liquid fixed point is preempted by Cooper pairing, such that for an initial  $\tilde{e} > 0$ , an attractive or repulsive four-fermion interaction in the BCS-channel eventually leads to superconductivity, enhanced by the coupling  $\tilde{e}$ . In a thin slice near  $(d = 5/2, m = 1)$ , the non-Fermi liquid fixed point is a stable fixed point. To reach the physical scenario with  $(d = 2, m = 1)$ , we have to set  $\varepsilon = 1/2$ , which is not quite

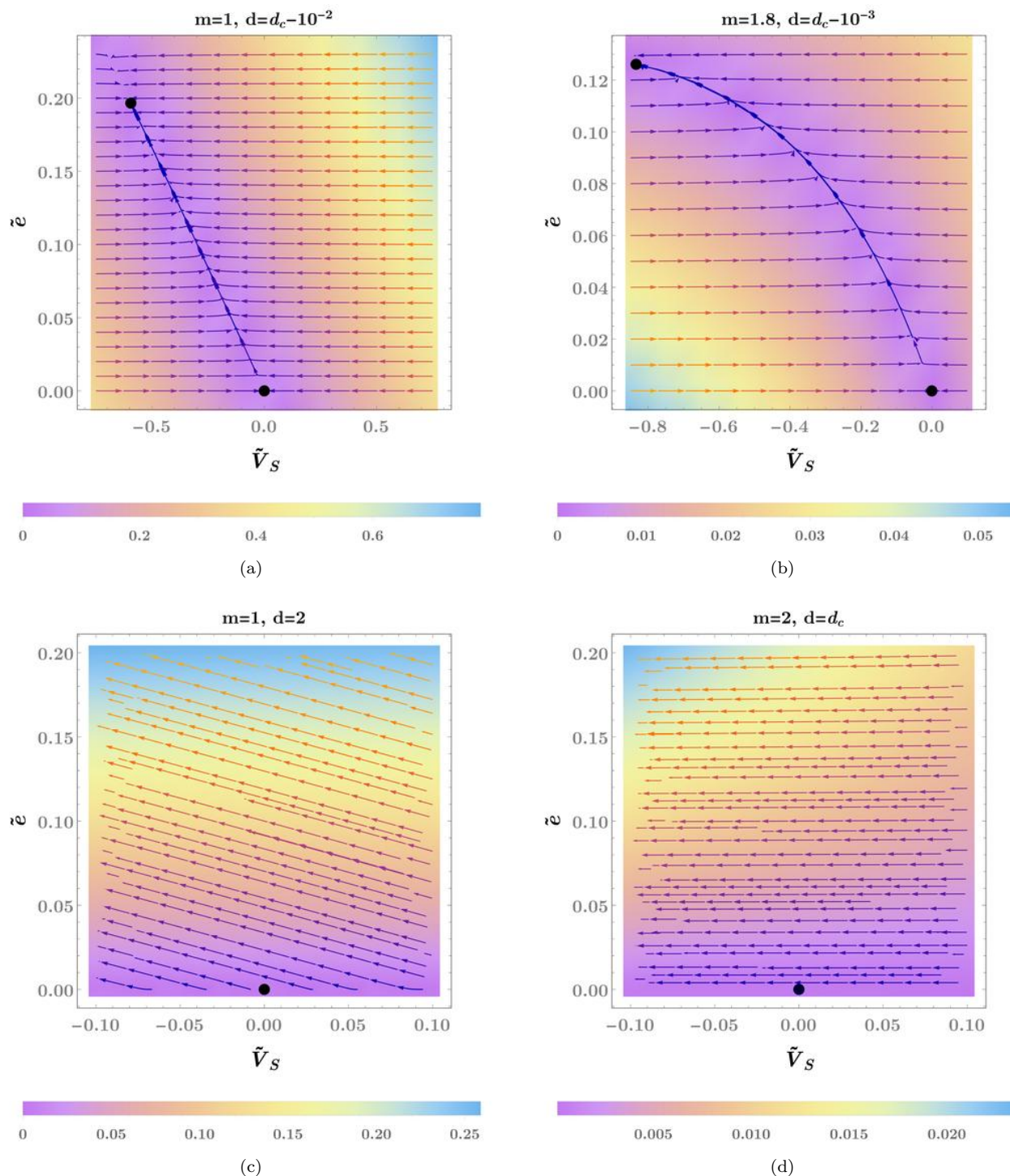


FIG. 9. The representative RG flows in the various regions of the  $(d, m)$ -plane. The black dots represent the finite fixed points when they exist. The contour-shading conveys the magnitudes of the flow vector  $\left(\frac{\partial \tilde{V}_S}{\partial l}, \frac{\partial \tilde{\epsilon}}{\partial l}\right)$  in different regions.

perturbatively controlled. However, if we extrapolate our results for  $\epsilon > 0.17$  to  $d = 2$ , then the  $(2+1)$ -d quantum critical point is expected to have strong enhancement of superconductivity by the order parameter fluctuations, such that even an initially repulsive  $\tilde{V}_S$  will eventually flow to the strong-coupling regime with large negative values.

Let us compare our results with previous works. In Ref. [48], the authors considered one-dimensional Fermi surfaces. In the present work, our formalism could treat both  $m = 1$  and  $m = 2$  Fermi surfaces. The  $(d = 2, m = 1)$  result agrees with that of Ref. [48]. The  $(d = 3, m = 2)$  result differs from the transverse gauge field case studied in Ref. [47], where the non-Fermi liquid arising from the interaction with a  $U(1)$  gauge field has been shown to give rise to pairing for angular momentum channels  $\ell \geq 2$  only when the gauge coupling is higher than a threshold value. The  $(d = 3, m = 2)$  Ising-

nematic case shows such pairing instability for all angular momentum channels and for any non-zero coupling constant  $\tilde{e}$ . This scenario persists even for a non-zero four-fermion pairing potential  $\tilde{V}_{S/A}$ .

Lastly, although we have considered the simplest case of zero angular momentum and two ( $N = 2$ ) flavours of fermions, our analysis can be easily extended to a scenario involving a non-zero angular momentum channel with any value of  $N$ . In future work, we would like to develop similar formalism for fermions coupled to transverse gauge fields, and also for SDW and CDW quantum critical points at which the critical bosons carry finite momenta.

### ACKNOWLEDGMENTS

We thank Sung-Sik Lee for suggesting this problem and for numerous helpful discussions. We are also grateful to Krishnendu Sengupta for providing valuable inputs in improving the manuscript. The research was supported by NSERC and the Templeton Foundation. Research at the Perimeter Institute is supported in part by the Government of Canada through Industry Canada, and by the Province of Ontario through the Ministry of Research and Information.

### Appendix A: Computation of the Feynman diagrams proportional to $V_S^2$

The diagrams resulting in terms proportional to  $V_S^2$  are shown in Fig. 2.

For  $\mathbf{p}_1 = \mathbf{p}_3$ , the contribution from Fig. 2a is proportional to:

$$\begin{aligned} I_1(\mathbf{P}_1 - \mathbf{P}_3) &= - \int dk \text{Tr}[G_0(k + \mathbf{P}_1 - \mathbf{P}_3) G_0(k)] \\ &= 2 \int dk \frac{\mathbf{K} \cdot (\mathbf{K} + \mathbf{P}_3 - \mathbf{P}_1) + \delta_k^2}{(\mathbf{K}^2 + \delta_k^2) [(\mathbf{K} + \mathbf{P}_3 - \mathbf{P}_1)^2 + \delta_k^2]} \exp\left(-\frac{2\mathbf{L}_{(k)}^2}{k_F}\right). \end{aligned} \quad (\text{A1})$$

Shifting the dummy variable  $k_{d-m} \rightarrow k_{d-m} + \mathbf{L}_{(k)}^2$  and using Feynman parametrization, we obtain:

$$\begin{aligned} I_1(\mathbf{P}_1 - \mathbf{P}_3) &= 2 \int dk \int_0^1 dt \frac{\mathbf{K} \cdot (\mathbf{K} + \mathbf{P}_3 - \mathbf{P}_1) + k_{d-m}^2}{[(1-t)(\mathbf{K}^2 + k_{d-m}^2) + t(\mathbf{K} + \mathbf{P}_3 - \mathbf{P}_1)^2 + t k_{d-m}^2]^2} \exp\left(-\frac{2\mathbf{L}_{(k)}^2}{k_F}\right) \\ &= 2 \int dk \int_0^1 dt \frac{\mathbf{K}^2 - t(1-t)(\mathbf{P}_3 - \mathbf{P}_1)^2 + k_{d-m}^2}{[\mathbf{K}^2 + k_{d-m}^2 + t(1-t)(\mathbf{P}_3 - \mathbf{P}_1)^2]^2} \exp\left(-\frac{2\mathbf{L}_{(k)}^2}{k_F}\right). \end{aligned} \quad (\text{A2})$$

In the last line, we have performed the variable shift  $\mathbf{K} \rightarrow \mathbf{K} - t(\mathbf{P}_3 - \mathbf{P}_1)$ . The remaining integrals can be computed in a straightforward manner to give:

$$I_1(\mathbf{P}_1 - \mathbf{P}_3) = \frac{2^{1-2d+\frac{m}{2}} k_F^{m/2} \pi^{1-\frac{d}{2}} \sec\left(\frac{(d-m)\pi}{2}\right) |\mathbf{P}_3 - \mathbf{P}_1|^{d-m-1}}{\Gamma\left(\frac{d-m}{2}\right)}, \quad (\text{A3})$$

which is logarithmically divergent at  $d - m = 1$ .

However, for  $\mathbf{p}_1 \neq \mathbf{p}_3$ , the contribution from Fig. 2a is proportional to:

$$\tilde{I}_1(p_1 - p_3) = - \int dk \text{Tr}[G_0(k + p_1 - p_3) G_0(k)] = -\beta_d \frac{|\mathbf{P}_1 - \mathbf{P}_3|^{d-m} k_F^{\frac{m-1}{2}}}{|\mathbf{L}_{(p_1-p_3)}|} \quad (\text{A4})$$

where  $\beta_d$  is defined in Eq. (5). This integral is the same as appears in the computation of the one-loop self-energy  $\Pi(q)$  for the bosonic propagator [22], and is convergent. So we must have  $\mathbf{p}_1 = \mathbf{p}_3$  to get a contribution to the RG equations.

For Fig. 2b, the contribution is proportional to:

$$I_2(p_2 - p_3) = - \int dk \text{Tr}[G_0(k + p_2 - p_3) G_0(k)] = \begin{cases} I_1(\mathbf{P}_2 - \mathbf{P}_3) & \text{for } |\mathbf{L}_{(p_2-p_3)}| \ll \frac{|\mathbf{P}_2 - \mathbf{P}_3|}{\sqrt{k_F}}, \\ \tilde{I}_1(p_2 - p_3) & \text{for } |\mathbf{L}_{(p_2-p_3)}| \gg \frac{|\mathbf{P}_2 - \mathbf{P}_3|}{\sqrt{k_F}}. \end{cases}$$

Performing the angular momentum decomposition, we get

$$\begin{aligned} &\int d\theta \theta^{m-1} I_2(p_2 - p_3) \\ &= \int_0^{\frac{|\mathbf{P}_2 - \mathbf{P}_3|}{\sqrt{k_F}}} d|\mathbf{L}_{(p_2-p_3)}| \frac{|\mathbf{L}_{(p_2-p_3)}|^{m-1} I_2(p_2 - p_3)}{k_F^{\frac{m}{2}}} + \int_{\frac{|\mathbf{P}_2 - \mathbf{P}_3|}{\sqrt{k_F}}}^{\infty} d|\mathbf{L}_{(p_2-p_3)}| \frac{|\mathbf{L}_{(p_2-p_3)}|^{m-1} I_2(p_2 - p_3)}{k_F^{\frac{m}{2}}} \\ &= \left\{ \frac{2^{1-2d+\frac{m}{2}} \pi^{1-\frac{d}{2}} \sec\left(\frac{(d-m)\pi}{2}\right)}{m \Gamma\left(\frac{d-m}{2}\right) k_F^{\frac{m}{2}}} + \frac{\beta_d}{m-1} \right\} \frac{|\mathbf{P}_2 - \mathbf{P}_3|^{d-1}}{k_F^{\frac{m}{2}}}, \end{aligned} \quad (\text{A5})$$

which is suppressed by  $1/k_F^m$  compared to the terms contributing to the beta functions.

In Fig. 2c, using the notation  $q_2 \equiv p_1 + p_2$ , we find that near  $d - m = 1$ , the terms resulting from the loop integral can be simplified and are proportional to

$$\begin{aligned}
& \int \left( \prod_{s=1}^4 dp_s \right) \delta^{(d+1)}(p_1 + p_2 - p_3 - p_4) \times \frac{1 - \delta_{j_1, j_2}}{(\mathbf{K}^2 + \delta_k^2) \left[ (\mathbf{K} - \mathbf{Q}_2)^2 + \delta_{k-q_2}^2 \right]} \\
& \times \sum_{j_1, j_2} \int d^{d-m} \mathbf{K} \left[ \{ \bar{\Psi}_{j_2}(p_3) \gamma_0 \Psi_{j_2}(p_2) \} \{ \bar{\Psi}_{j_1}(p_4) \gamma_0 \Psi_{j_1}(p_1) \} \mathbf{K} \cdot (\mathbf{Q}_2 - \mathbf{K}) \right. \\
& \quad \left. + \{ \bar{\Psi}_{j_2}(p_3) \gamma_{d-m} \Psi_{j_2}(p_2) \} \{ \bar{\Psi}_{j_1}(p_4) \gamma_{d-m} \Psi_{j_1}(p_1) \} \delta_k \delta_{k-q_2} \right] \\
& + \text{terms not contributing to Cooper pairing} \\
& = 2 \int \left( \prod_{s=1}^4 dp_s \right) \delta^{(d+1)}(p_1 + p_2 - p_3 - p_4) \sum_{j_1, j_2} \psi_{+, j_2}^\dagger(p_3) \psi_{-, j_1}^\dagger(-p_1) \psi_{-, j_1}(-p_4) \psi_{+, j_2}(-p_3) (1 - \delta_{j_1, j_2}) \\
& \quad \times I_3(q_2) + \text{terms not contributing to Cooper pairing},
\end{aligned}$$

where

$$I_3(q_2) = \int d^{d-m} \mathbf{K} \frac{\mathbf{K} \cdot (\mathbf{Q}_2 - \mathbf{K}) + \delta_k \delta_{k-q_2}}{(\mathbf{K}^2 + \delta_k^2) \left[ (\mathbf{K} - \mathbf{Q}_2)^2 + \delta_{k-q_2}^2 \right]} \exp \left( -\frac{2 \mathbf{L}_{(k)}^2}{k_F} \right) = I_2(q_2), \tag{A6}$$

which therefore do not contribute to the RG-flow.

### Appendix B: One-loop diagrams proportional to $\tilde{e} V_S$

The first set of diagrams generating terms proportional to  $e^2 V_S$  is shown in Fig. 4. We will use  $M$  to denote the matrices belonging to the set  $\{\sigma_z, \mathbb{I}_{2 \times 2}\}$ .

The term arising from Fig. 4a is given by:

$$\begin{aligned}
& t_M^1(p_1, p_2, p_3) \\
& = -\frac{V_S (ie)^2 \mu^{x+d_v}}{4N} (1 - \delta_{j_1, j_2}) \times \frac{2}{2!} \\
& \quad \times \int dk D_1(k) \{ \bar{\Psi}_{j_1}(p_3) M \gamma_{d-m} G_0(p_3 - k) G_0(p_1 - k) \gamma_{d-m} \Psi_{j_2}(p_1) \} \{ \bar{\Psi}_{j_2}(p_4) M \Psi_{j_1}(p_2) \} \\
& = -\frac{V_S e^2 \mu^{x+d_v} (1 - \delta_{j_1, j_2})}{4N} \{ \bar{\Psi}_{j_1}(p_3) M \Psi_{j_2}(p_1) \} \{ \bar{\Psi}_{j_2}(p_4) M \Psi_{j_1}(p_2) \} J_1, \tag{B1}
\end{aligned}$$

where

$$\begin{aligned}
J_1 & = i^2 \int dk \gamma_{d-m} G_0(p_3 - k) G_0(p_1 - k) \gamma_{d-m} D_1(k) \\
& = \int dk \frac{(\mathbf{K} + \mathbf{P}_1) \cdot (\mathbf{K} + \mathbf{P}_3) + \delta_{k+p_1}^2}{\{(\mathbf{K} + \mathbf{P}_1)^2 + \delta_{k+p_1}^2\} \{(\mathbf{K} + \mathbf{P}_3)^2 + \delta_{k+p_1}^2\} [\mathbf{L}_{(k)}^2 + \tilde{\alpha} \frac{|\mathbf{K}|^{d-m}}{|\mathbf{L}_{(k)}|}]} . \tag{B2}
\end{aligned}$$

Shifting  $k_{d-m} \rightarrow (k - p_1)_{d-m} - \mathbf{L}_{(k+p_1)}^2$ ,  $\mathbf{K} \rightarrow \mathbf{K} - \mathbf{P}_3$ , and performing the  $\mathbf{L}_{(k)}$ -integral, we get

$$\begin{aligned}
J_1 & = \frac{|\csc\{\frac{(m+1)\pi}{3}\}| \pi^{\frac{m}{2}}}{3 \Gamma(\frac{m}{2}) \tilde{\alpha}^{\frac{2-m}{3}}} \int \frac{d^{d-m} \mathbf{K} dk_{d-m}}{(2\pi)^d} \frac{\mathbf{K} \cdot (\mathbf{K} + \mathbf{Q}_3) + k_{d-m}^2}{\{(\mathbf{K} + \mathbf{Q})^2 + k_{d-m}^2\} \{\mathbf{K}^2 + k_{d-m}^2\} |\mathbf{K} - \mathbf{P}_3|^{2\beta}} \\
& \simeq \frac{|\csc(\frac{\delta\pi}{3})| \pi^{\frac{m}{2}}}{3 \Gamma(\frac{m}{2}) \tilde{\alpha}^{\frac{\delta}{3}}} \int_0^1 dt \int \frac{d^{d-m} \mathbf{K} dk_{d-m}}{(2\pi)^d |\mathbf{K}|^{2\beta}} \frac{\mathbf{K} \cdot (\mathbf{K} + \mathbf{Q}_3) + k_{d-m}^2}{\{t(\mathbf{K} + \mathbf{Q}_3)^2 + (1-t)\mathbf{K}^2 + k_{d-m}^2\}^2} \left[ 1 + \frac{\delta(d-2+\delta) \mathbf{K} \cdot \mathbf{P}_3}{3 \mathbf{K}^2} \right] \\
& = \frac{|\csc(\frac{\delta\pi}{3})| \pi^{1+\frac{m}{2}}}{6 \Gamma(\frac{m}{2}) \tilde{\alpha}^{\frac{\delta}{3}}} \int_0^1 dt \int \frac{d^{d-m} \mathbf{K}}{(2\pi)^d |\mathbf{K}|^{2\beta}} \frac{\mathbf{K} \cdot (\mathbf{K} + \mathbf{Q}_3) + t(\mathbf{K} + \mathbf{Q}_3)^2 + (1-t)\mathbf{K}^2}{\{t(\mathbf{K} + \mathbf{Q}_3)^2 + (1-t)\mathbf{K}^2\}^{\frac{3}{2}}} \\
& \quad \times \left[ 1 + \frac{\delta(d-2+\delta) \mathbf{K} \cdot \mathbf{P}_3}{3 \mathbf{K}^2} \right], \tag{B3}
\end{aligned}$$

where

$$\mathbf{Q}_3 = \mathbf{P}_1 - \mathbf{P}_3, \beta = \frac{(d-m)(2-m)}{6}, m = 2 - \delta, d = m + \frac{3}{m+1} - \varepsilon. \quad (\text{B4})$$

such that  $\varepsilon = \varepsilon(1 - \frac{\delta}{3})$ . We have expanded the expression in terms of small  $\mathbf{P}_3$ , which enables us to analyse the singularity structure without any loss of generality. Defining  $\mathcal{D} = \mathbf{K}^2 + t(1-y)(1-t+yt)\mathbf{Q}_3^2$ , we get

$$\begin{aligned} J_1 &= \frac{|\csc(\frac{\delta\pi}{3})| \pi^{1+\frac{m}{2}} \Gamma(\beta + \frac{3}{2})}{6 \Gamma(\frac{m}{2}) \tilde{\alpha}^{\frac{6}{3}} \Gamma(\beta) \Gamma(\frac{3}{2})} \int_0^1 dy \int_0^1 dt \int \frac{d^{d-m}\mathbf{K}}{(2\pi)^d} \frac{2\mathbf{K}^2 + yt(1-2t+2yt)\mathbf{Q}_3^2}{\mathcal{D}^{\beta+\frac{3}{2}}} y^{\beta-1} \sqrt{1-y} \\ &\quad \times \left[ 1 - \frac{(2\beta+3)t^2(1-y)\mathbf{Q}_3 \cdot \mathbf{P}_3}{\mathcal{D}} \right] \\ &= \frac{|\csc(\frac{\delta\pi}{3})|}{6 \tilde{\alpha}^{\frac{6}{3}} (2\pi)^{\frac{3}{3+\delta} - \delta} \Gamma(1 - \frac{\delta}{2}) \Gamma(\frac{3}{6-2\delta}) \varepsilon(1 - \frac{\delta}{3}) |\mathbf{Q}_3|^{\varepsilon(1 - \frac{\delta}{3})}} 1 + \mathcal{O}(1). \end{aligned} \quad (\text{B5})$$

This is logarithmically divergent at  $d = d_c$ . Near  $(d = 3, m = 2)$ , we expand in small delta such that

$$J_1 = \frac{1}{4\pi^2} \frac{1}{\delta \varepsilon (1 - \frac{\delta}{3}) |\mathbf{Q}_3|^{\varepsilon(1 - \frac{\delta}{3})}} + \mathcal{O}(1). \quad (\text{B6})$$

This indicates there is a  $\log^2$  divergence. We note that there is no  $\mathbf{P}_3$ -dependent term divergent in  $\frac{1}{\delta}$  or  $\frac{1}{\varepsilon(1 - \frac{\delta}{3})}$ . In fact, the leading order term dependent on  $\mathbf{P}_3$  goes as  $\frac{1-2\ln 2}{4\pi^5} \frac{\mathbf{Q}_3 \cdot \mathbf{P}_3}{|\mathbf{Q}_3|^{2+\varepsilon(1 - \frac{\delta}{3})}}$ .

The term arising from Fig. 4b has a divergent structure identical to Fig. 4a. Depending on  $m$ , these two diagrams are of either higher order than or same order as the  $V_S^2$  terms. Near  $(d = 5/2, m = 1)$ , these have only a pole in  $\varepsilon$  (and not in  $\delta$ ) and hence are of leading order. On the other hand, near  $(d = 3, m = 2)$ , these have two poles (one in  $\varepsilon$  and one in  $\delta$ ) and hence are one order higher than the  $V_S^2$  terms. In this second scenario, namely near  $(d = 3, m = 2)$ , these two diagrams must then be considered in conjunction with those consisting of the counterterm vertices generated from the divergence of the angular momentum decomposition of Fig. 3, as shown in Fig. 5. In Sec. B1, we have shown how these terms cancel out around this region.

The term arising from Fig. 4c is given by:

$$\begin{aligned} &t_M^3(p_1, p_2, p_3) \\ &= -\frac{V_S (ie)^2 \mu^{x+d_v}}{4N} (1 - \delta_{j_1, j_2}) \\ &\quad \times \int dk D_1(k - p_3) \{ \bar{\Psi}_{j_1}(p_3) \gamma_{d-m} G_0(k) M \Psi_{j_2}(p_1) \} \{ \bar{\Psi}_{j_2}(p_4) \gamma_{d-m} G_0(p_1 + p_2 - k) M \Psi_{j_1}(p_2) \} \\ &\simeq -\frac{V_S e^2 \mu^{x+d_v}}{4N} (1 - \delta_{j_1, j_2}) \{ \bar{\Psi}_{j_1}(p_3) M \Psi_{j_2}(p_1) \} \{ \bar{\Psi}_{j_2}(p_4) M \Psi_{j_1}(p_2) \} J_3, \end{aligned} \quad (\text{B7})$$

where we have dropped terms irrelevant for superconductivity such that

$$J_3 = - \int dk \frac{\mathbf{K} \cdot (\mathbf{K} - \mathbf{P}_1 - \mathbf{P}_2) - \delta_k \delta_{k-p_1-p_2}}{\{ \mathbf{K}^2 + \delta_k^2 \} \{ (\mathbf{K} - \mathbf{P}_1 - \mathbf{P}_2)^2 + \delta_{k-p_1-p_2}^2 \} [\mathbf{L}_{(k-p_3)}^2 + \tilde{\alpha} \frac{|\mathbf{K} - \mathbf{P}_3|^{d-m}}{|\mathbf{L}_{(k-p_3)}|}]} = 0, \quad (\text{B8})$$

on performing the  $k_{d-m}$  integral. Similarly, the contribution from Fig. 4d also vanishes.

Next we consider Fig. 4e, again only keeping terms relevant for superconductivity. This contributes as:

$$\begin{aligned} &t_M^5(p_1, p_2, p_3) \\ &= -\frac{V_S (ie)^2 \mu^{x+d_v}}{4N} (1 - \delta_{j_1, j_2}) \\ &\quad \times \int dk D_1(k) \{ \bar{\Psi}_{j_1}(p_3) M G_0(p_1 - k) \gamma_{d-m} \Psi_{j_2}(p_1) \} \{ \bar{\Psi}_{j_2}(p_4) \gamma_{d-m} G_0(p_4 - k) M \Psi_{j_1}(p_2) \} \\ &\simeq -\frac{V_S e^2 \mu^{x+d_v}}{4N} (1 - \delta_{j_1, j_2}) \{ \bar{\Psi}_{j_1}(p_3) M \Psi_{j_2}(p_1) \} \{ \bar{\Psi}_{j_2}(p_4) M \Psi_{j_1}(p_2) \} J_5, \end{aligned} \quad (\text{B9})$$

where

$$\begin{aligned} J_5 &= \int dk \frac{(\mathbf{K} - \mathbf{P}_1) \cdot (\mathbf{K} - \mathbf{P}_4) + \delta_{k-p_1} \delta_{k-p_4}}{\{ (\mathbf{K} - \mathbf{P}_1)^2 + \delta_{k-p_1}^2 \} \{ (\mathbf{K} - \mathbf{P}_4)^2 + \delta_{k-p_4}^2 \} [\mathbf{L}_{(k)}^2 + \tilde{\alpha} \frac{|\mathbf{K}|^{d-m}}{|\mathbf{L}_{(k)}|}]} \\ &= \int dk \frac{\mathbf{K} \cdot (\mathbf{K} + \mathbf{P}_1 - \mathbf{P}_4) + \delta_{k+p_1} \delta_{k+p_2}}{\{ \mathbf{K}^2 + \delta_{k+p_1}^2 \} \{ (\mathbf{K} + \mathbf{P}_1 - \mathbf{P}_4)^2 + \delta_{k+p_2}^2 \} [\mathbf{L}_{(k)}^2 + \tilde{\alpha} \frac{|\mathbf{K} + \mathbf{P}_1|^{d-m}}{|\mathbf{L}_{(k)}|}]} . \end{aligned}$$

Setting  $\mathbf{p}_1 (= \mathbf{p}_3) = 0$  and  $\mathbf{P}_1 = \mathbf{P}_4$  for simplification, which is valid for extracting the divergent term, we get:

$$\begin{aligned} J_5 &= \int dk \frac{\mathbf{K}^2 + \delta_k \delta_{k+p_2}}{\{\mathbf{K}^2 + \delta_k^2\} \{\mathbf{K}^2 + \delta_{k+p_2}^2\} [\mathbf{L}_{(k)}^2 + \tilde{\alpha} \frac{|\mathbf{K} + \mathbf{P}_1|^{d-m}}{|\mathbf{L}_{(k)}|}]} \\ &= \frac{1}{\pi (2\pi)^d} \int \frac{d^{d-m} \mathbf{K} d^m \mathbf{L}_{(k)} |\mathbf{K}|}{\{\mathbf{K}^2 + \mathbf{L}_{(k)}^2 \mathbf{L}_{(p_2)}^2 \cos^2 \theta_k\} [\mathbf{L}_{(k)}^2 + \tilde{\alpha} \frac{|\mathbf{K} + \mathbf{P}_1|^{d-m}}{|\mathbf{L}_{(k)}|}]} . \end{aligned}$$

In the last step, we have ignored the terms involving  $\delta_{p_2}$  in the denominator, and used  $\theta_k$  to denote the angle between  $\mathbf{L}_{(k)}$  and  $\mathbf{L}_{(p_2)}$ .

In order to proceed further and obtain an analytic expression, we need to examine which terms in the integral lead to singularity. If  $k = (\mathbf{K}, k_{d-m}, \mathbf{L}_{(k)})$  denotes the momentum flowing through a boson propagator within a loop diagram, such that  $|\mathbf{K}|$  is order of  $\Lambda$ , the typical momentum carried by a boson along the tangential direction of the Fermi surface is given by  $|\mathbf{L}_{(k)}|^3 \sim \tilde{\alpha} \Lambda^{d-m}$ . For a fixed value of  $\tilde{\epsilon} \sim \mathcal{O}(\epsilon)$ , we can neglect the first term for  $\tilde{\alpha}^{\frac{1}{3}} \Lambda^{\frac{d-m}{3}} |\mathbf{L}_{(p_2)}| \gg \Lambda$ , and the second term for  $\alpha^{\frac{1}{3}} \Lambda^{\frac{d-m}{3}} |\mathbf{L}_{(p_2)}| \ll \Lambda$ , in the  $\{\mathbf{K}^2 + \mathbf{L}_{(k)}^2 \mathbf{L}_{(p_2)}^2 \cos^2 \theta_k\}$  factor of the denominator [23]. This gives us

$$J_5 = \begin{cases} \int d^{d-m} \mathbf{K} \frac{\pi^{\frac{7-2d-\delta}{2}} \csc(\frac{\delta-1}{3}\pi) \sec(\frac{\delta\pi}{2}) |\mathbf{K}|}{3 \times 2^{d-1+\delta} \Gamma(-\delta) \Gamma(\frac{1+\delta}{2}) \mathbf{L}_{(p_2)}^2 |\mathbf{K} + \mathbf{P}_1|^{\frac{(2+\delta)(d-2+\delta)}{3}} \tilde{\alpha}^{\frac{2+\delta}{3}}} & \text{for } \tilde{\alpha}^{\frac{1}{3}} \Lambda^{\frac{d-m}{3}} |\mathbf{L}_{(p_2)}| \gg \Lambda, \\ \int d^{d-m} \mathbf{K} \frac{\pi^{\frac{4-2d+m}{2}} \csc(\frac{m+1}{3}\pi)}{3 \times 2^{d-1} \Gamma(\frac{m}{2}) |\mathbf{K}| |\mathbf{K} + \mathbf{P}_1|^{\frac{(d-m)(2-m)}{3}} \tilde{\alpha}^{\frac{2-m}{3}}} & \text{for } \tilde{\alpha}^{\frac{1}{3}} \Lambda^{\frac{d-m}{3}} |\mathbf{L}_{(p_2)}| \ll \Lambda, \end{cases}$$

where  $\delta = 2 - m$ . Finally, performing the  $\mathbf{K}$  integrals, the leading order terms are found to be:

$$J_5 = \begin{cases} \sqrt{3} |\mathbf{P}_1| \frac{4 - (1 - \frac{\delta}{3}) \epsilon - 2\delta + (1 - \frac{\delta}{3}) \epsilon \delta}{3 - \delta} \delta & \text{for } \tilde{\alpha}^{\frac{1}{3}} \Lambda^{\frac{d-m}{3}} |\mathbf{L}_{(p_2)}| \gg \Lambda, \\ \frac{4 \tilde{\alpha}^{\frac{2+\delta}{3}} \mathbf{L}_{(p_2)}^2}{\pi^{2 - \frac{m}{2} - \frac{3}{2(m+1)}} \csc(\frac{m+1}{3}\pi)} \frac{1}{2 |\mathbf{P}_1|^{\frac{(m+1)\epsilon}{3}} \epsilon} & \text{for } \tilde{\alpha}^{\frac{1}{3}} \Lambda^{\frac{d-m}{3}} |\mathbf{L}_{(p_2)}| \ll \Lambda . \end{cases} \quad (\text{B10})$$

Now we need to carry out the angular momentum decomposition to get

$$\begin{aligned} e^2 \int d\theta \theta^{m-1} J_5 &= e^2 \int_0^{\frac{\Lambda^{\frac{3-d+m}{3}}}{\tilde{\alpha}^{\frac{1}{3}}}} d|\mathbf{L}_{(p_2)}| \frac{|\mathbf{L}_{(p_2)}|^{m-1} J_5}{k_F^{\frac{m}{2}}} + e^2 \int_{\frac{\Lambda^{\frac{3-d+m}{3}}}{\tilde{\alpha}^{\frac{1}{3}}}}^{\infty} d|\mathbf{L}_{(p_2)}| \frac{|\mathbf{L}_{(p_2)}|^{m-1} J_5}{k_F^{\frac{m}{2}}} \\ &= \frac{\pi^{2 - \frac{m}{2} - \frac{3}{2(m+1)}} \csc(\frac{m+1}{3}\pi)}{2^{\frac{2+m^2}{m+1}} (m+1) \Gamma(\frac{m+2}{2}) \Gamma(\frac{3}{2(m+1)})} \tilde{\alpha}^{\frac{2}{3}} |\mathbf{P}_1|^{\frac{(m+1)\epsilon}{3}} k_F^{\frac{m}{2}} \epsilon + \frac{\sqrt{3} |\mathbf{P}_1|^{\frac{4 - (1 - \frac{\delta}{3}) \epsilon - 2\delta + (1 - \frac{\delta}{3}) \epsilon \delta}{3 - \delta}}}{4 \tilde{\alpha}^{\frac{2}{3}}} \frac{e^2}{\Lambda^{\frac{(3-d+m)\delta}{3}} k_F^{\frac{m}{2}}}, \end{aligned} \quad (\text{B11})$$

which is suppressed by an overall factor of  $\tilde{\epsilon}^{\frac{1}{m+1}} / k_F^{\frac{m^2}{m+1}}$ . Hence, this diagram is not relevant for the RG-equations. It is easy to see that Fig. 4f has the same singularity behaviour as Fig. 4e.

### 1. Cancellation of the terms proportional to $\tilde{\epsilon} \tilde{V}_S$ near $m = 2$

The  $\log^2$  divergences in the diagrams in Fig. 4 near  $m = 2$  need to be examined carefully, as potentially they can give rise to non-local terms in the renormalized action. For  $m = 2 - \delta$  and  $d = d_c - \epsilon$ , the diagram in Fig. 4a, for example, diverges as

$$-\frac{2 \tilde{\epsilon} \tilde{V}_S}{4N} J_1 = \frac{\tilde{\epsilon} \tilde{V}_S}{8\pi^2 N} \left[ -\frac{1}{\delta \epsilon (1 - \frac{\delta}{3})} + \frac{\ln\left(\frac{|\mathbf{P}_1 - \mathbf{P}_3|}{\mu}\right)}{\delta} + \frac{\gamma_E}{\epsilon (1 - \frac{\delta}{3})} + \frac{\gamma_E}{\delta} \right], \quad (\text{B12})$$

where  $\gamma_E = 0.577$  is the Euler-Mascheroni constant. The above must be considered in conjunction with the diagram in Fig. 5a, which gives a divergent term equal to

$$\frac{2 \times 2 \tilde{\epsilon} \tilde{V}_S}{4} \frac{1}{N} \frac{1}{2^{\frac{3m}{2}} \pi^{1+\frac{m}{2}}} \left[ \frac{1 - \gamma_E \ln\left(\frac{|\mathbf{P}_1 - \mathbf{P}_3|}{\mu}\right)}{\delta \gamma_E} - \frac{\gamma_E}{\gamma \epsilon} + \frac{\gamma_E}{\delta} \right] = \frac{\tilde{\epsilon} \tilde{V}_S}{8\pi^2 N} \left[ \frac{1}{\delta \gamma \epsilon} - \frac{\ln\left(\frac{|\mathbf{P}_1 - \mathbf{P}_3|}{\mu}\right)}{\delta} - \frac{\gamma_E}{\gamma \epsilon} + \frac{\gamma_E}{\delta} \right]. \quad (\text{B13})$$

Clearly, the coefficients of  $\ln\left(\frac{|\mathbf{P}_1-\mathbf{P}_3|}{\mu}\right)$  cancel and there is no dangerous non-local term in the renormalized action. Moreover, the  $\log^2$  divergence at  $(d=3, m=2)$  also cancels out (with  $\gamma=1$ ), as expected in the minimal subtraction scheme.

### Appendix C: Treatment of the terms proportional to $\tilde{\epsilon}$ in the Wilsonian RG language

From our boson propagator  $D_1(q)$ , it is clear that the instantaneous interaction is mediated by bosons with momenta  $|\mathbf{L}_{(q)}| \gtrsim \lambda_t \equiv e^{2/3}\beta_d^{1/3}\Lambda^{\frac{d-m+x}{3}}k_F^{\frac{m-1}{6}}$ . In the words of Son [46], *part of the non-instantaneous interaction becomes instantaneous* when RG is carried out with  $e^{-\frac{(4-m)l}{6}}\lambda_t < |\mathbf{L}_{(q)}| < \lambda_t$ . Here we note that since we are using the *dressed* bosonic propagator, this is the correct interval to be considered. On the other hand, in the analysis of Metlitski *et al.* [48], since the cut-off in the tangential direction is proportional to  $\sqrt{\Lambda k_F}$ , RG is carried out with  $e^{\frac{l}{2}}\sqrt{\Lambda k_F} < |\mathbf{L}_{(q)}| < \sqrt{\Lambda k_F}$ . These two approaches match for  $m=1$ . It is more logical to integrate out the instantaneous part of the boson propagator with  $|\mathbf{L}_{(q)}|$  in the appropriate range obtained following Son's approach [46]. Moreover, for  $m > 1$ , there is an already non-trivial  $k_F$  dependence from UV-IR mixing arising due to inter-patch coupling, caused by the interactions with the massless boson [22]. We conclude that in the presence of the four-fermion interactions, the UV-IR mixing becomes manifest even for  $m=1$ .

Setting  $\mathbf{P}_1 = \mathbf{P}_2$  gives the ‘‘instantaneous’’ contribution in the BCS-channel with angular momentum  $\ell$ , which can be expressed as:

$$t_{ee}(l, \ell) = \begin{cases} \frac{e^2 \Lambda^x}{2N} \times 2 \int_{\theta>0} \frac{d\theta}{2\pi} \frac{e^{-i\ell\theta}}{\mathbf{L}_{(q)}^2} & \text{for } m=1, \\ \frac{e^2 \Lambda^x}{4N} \int d\theta \frac{\sin\theta P_\ell(\cos\theta)}{\mathbf{L}_{(q)}^2} & \text{for } m=2. \end{cases} \quad (\text{C1})$$

Using  $\epsilon = m + 1 - d$ , we get

$$t_{ee}(l, \ell) \simeq \begin{cases} \frac{e^2 \Lambda^x}{2N\pi} \int_{e^{-\frac{l}{2}}\lambda_t}^{\lambda_t} d|\mathbf{L}_{(q)}| \frac{1}{\sqrt{k_F} \mathbf{L}_{(q)}^2} = \frac{e^2 \Lambda^x}{2N\pi\sqrt{k_F}\lambda_t} \frac{l}{2} = \frac{\tilde{\epsilon}\Lambda^\epsilon}{N\sqrt{k_F}\beta_d^{1/3}} \frac{l}{4\pi} & \text{for } m=1, \\ \frac{e^2 \Lambda^x}{4N} \int_{e^{-\frac{l}{3}}\lambda_t}^{\lambda_t} d|\mathbf{L}_{(q)}| \frac{P_\ell(1)}{k_F |\mathbf{L}_{(q)}|} = \frac{\tilde{\epsilon}\Lambda^\epsilon}{4Nk_F} \frac{l}{3} & \text{for } m=2, \end{cases} \quad (\text{C2})$$

which is independent of the angular momentum channel  $\ell$ .

- 
- [1] T. Holstein, R. E. Norton, and P. Pincus, de Haas-van Alphen effect and the specific heat of an electron gas, *Phys. Rev. B* **8**, 2649 (1973).
- [2] M. Y. Reizer, Relativistic effects in the electron density of states, specific heat, and the electron spectrum of normal metals, *Phys. Rev. B* **40**, 11571 (1989).
- [3] P. A. Lee and N. Nagaosa, Gauge theory of the normal state of high- $T_c$  superconductors, *Phys. Rev. B* **46**, 5621 (1992).
- [4] B. I. Halperin, P. A. Lee, and N. Read, Theory of the half-filled Landau level, *Phys. Rev. B* **47**, 7312 (1993).
- [5] J. Polchinski, Low-energy dynamics of the spinon-gauge system, *Nuclear Physics B* **422**, 617 (1994).
- [6] B. L. Altshuler, L. B. Ioffe, and A. J. Millis, Low-energy properties of fermions with singular interactions, *Phys. Rev. B* **50**, 14048 (1994).
- [7] E.-A. Kim, M. J. Lawler, P. Oreto, S. Sachdev, E. Fradkin, and S. A. Kivelson, Theory of the nodal nematic quantum phase transition in superconductors, *Phys. Rev. B* **77**, 184514 (2008).
- [8] C. Nayak and F. Wilczek, Renormalization group approach to low temperature properties of a non-Fermi liquid metal, *Nuclear Physics B* **430**, 534 (1994).
- [9] M. J. Lawler, D. G. Barci, V. Fernández, E. Fradkin, and L. Oxman, Nonperturbative behavior of the quantum phase transition to a nematic Fermi fluid, *Phys. Rev. B* **73**, 085101 (2006).
- [10] M. J. Lawler and E. Fradkin, Local quantum criticality at the nematic quantum phase transition, *Phys. Rev. B* **75**, 033304 (2007).
- [11] S.-S. Lee, Low-energy effective theory of Fermi surface coupled with U(1) gauge field in 2 + 1 dimensions, *Phys. Rev. B* **80**, 165102 (2009).
- [12] M. A. Metlitski and S. Sachdev, Quantum phase transitions of metals in two spatial dimensions. I. Ising-nematic order, *Phys. Rev. B* **82**, 075127 (2010).
- [13] M. A. Metlitski and S. Sachdev, Quantum phase transitions of metals in two spatial dimensions. II. Spin density wave order, *Phys. Rev. B* **82**, 075128 (2010).
- [14] A. Abanov and A. Chubukov, Anomalous scaling at the quantum critical point in itinerant antiferromagnets, *Physical Review Letters* **93**, 255702 (2004).
- [15] A. Abanov and A. V. Chubukov, Spin-fermion model near the quantum critical point: One-loop renormalization group results, *Physical Review Letters* **84**, 5608 (2000).

- [16] A. Abanov, A. V. Chubukov, and J. Schmalian, Quantum-critical theory of the spin-fermion model and its application to cuprates: normal state analysis, *Advances in Physics* **52**, 119 (2003).
- [17] D. F. Mross, J. McGreevy, H. Liu, and T. Senthil, Controlled expansion for certain non-Fermi-liquid metals, *Phys. Rev. B* **82**, 045121 (2010).
- [18] H.-C. Jiang, M. S. Block, R. V. Mishmash, J. R. Garrison, D. N. Sheng, O. I. Motrunich, and M. P. A. Fisher, Non-Fermi-liquid d-wave metal phase of strongly interacting electrons, *Nature (London)* **493**, 39 (2013).
- [19] S. Sur and S.-S. Lee, Chiral non-Fermi liquids, *Phys. Rev. B* **90**, 045121 (2014).
- [20] D. Dalidovich and S.-S. Lee, Perturbative non-Fermi liquids from dimensional regularization, *Phys. Rev. B* **88**, 245106 (2013).
- [21] S. Sur and S.-S. Lee, Quasilocally strange metal, *Phys. Rev. B* **91**, 125136 (2015).
- [22] I. Mandal and S.-S. Lee, Ultraviolet/infrared mixing in non-Fermi liquids, *Phys. Rev. B* **92**, 035141 (2015).
- [23] I. Mandal, UV/IR mixing in non-Fermi liquids: Higher-loop corrections in different energy ranges, *European Physical Journal B* **89**, 278 (2016).
- [24] A. Eberlein, I. Mandal, and S. Sachdev, Hyperscaling violation at the Ising-nematic quantum critical point in two-dimensional metals, *Phys. Rev. B* **94**, 045133 (2016).
- [25] V. Oganesyan, S. A. Kivelson, and E. Fradkin, Quantum theory of a nematic Fermi fluid, *Phys. Rev. B* **64**, 195109 (2001).
- [26] W. Metzner, D. Rohe, and S. Andergassen, Soft Fermi Surfaces and Breakdown of Fermi-Liquid Behavior, *Phys. Rev. Lett.* **91**, 066402 (2003).
- [27] L. Dell'Anna and W. Metzner, Fermi surface fluctuations and single electron excitations near Pomeranchuk instability in two dimensions, *Phys. Rev. B* **73**, 045127 (2006).
- [28] L. Dell'Anna and W. Metzner, Electrical resistivity near Pomeranchuk instability in two dimensions, *Phys. Rev. Lett.* **98**, 136402 (2007).
- [29] H.-Y. Kee, E. H. Kim, and C.-H. Chung, Signatures of an electronic nematic phase at the isotropic-nematic phase transition, *Phys. Rev. B* **68**, 245109 (2003).
- [30] J. Rech, C. Pépin, and A. V. Chubukov, Quantum critical behavior in itinerant electron systems: Eliashberg theory and instability of a ferromagnetic quantum critical point, *Phys. Rev. B* **74**, 195126 (2006).
- [31] P. Wölfle and A. Rosch, Fermi liquid near a quantum critical point, *Journal of Low Temperature Physics* **147**, 165 (2007).
- [32] D. L. Maslov and A. V. Chubukov, Fermi liquid near Pomeranchuk quantum criticality, *Phys. Rev. B* **81**, 045110 (2010).
- [33] J. Quintanilla and A. J. Schofield, Pomeranchuk and topological Fermi surface instabilities from central interactions, *Phys. Rev. B* **74**, 115126 (2006).
- [34] H. Yamase and H. Kohno, Instability toward formation of quasi-one-dimensional Fermi surface in two-dimensional t-J model, *Journal of the Physical Society of Japan* **69**, 2151 (2000).
- [35] H. Yamase, V. Oganesyan, and W. Metzner, Mean-field theory for symmetry-breaking Fermi surface deformations on a square lattice, *Phys. Rev. B* **72**, 035114 (2005).
- [36] C. J. Halboth and W. Metzner, d-wave superconductivity and Pomeranchuk instability in the two-dimensional Hubbard model, *Phys. Rev. Lett.* **85**, 5162 (2000).
- [37] P. Jakubczyk, P. Strack, A. A. Katanin, and W. Metzner, Renormalization group for phases with broken discrete symmetry near quantum critical points, *Phys. Rev. B* **77**, 195120 (2008).
- [38] M. Zacharias, P. Wölfle, and M. Garst, Multiscale quantum criticality: Pomeranchuk instability in isotropic metals, *Phys. Rev. B* **80**, 165116 (2009).
- [39] Y. Huh and S. Sachdev, Renormalization group theory of nematic ordering in d-wave superconductors, *Phys. Rev. B* **78**, 064512 (2008).
- [40] O. I. Motrunich, Variational study of triangular lattice spin-1/2 model with ring exchanges and spin liquid state in  $\kappa$ -( $\text{ET}$ )<sub>2</sub>Cu<sub>2</sub>(CN)<sub>3</sub>, *Phys. Rev. B* **72**, 045105 (2005).
- [41] S.-S. Lee and P. A. Lee, U(1) gauge theory of the Hubbard model: Spin liquid states and possible application to  $\kappa$ -(BEDT-TTF)<sub>2</sub>Cu<sub>2</sub>(CN)<sub>3</sub>, *Phys. Rev. Lett.* **95**, 036403 (2005).
- [42] P. A. Lee, N. Nagaosa, and X.-G. Wen, Doping a Mott insulator: Physics of high-temperature superconductivity, *Reviews of Modern Physics* **78**, 17 (2006).
- [43] O. I. Motrunich and M. P. A. Fisher, d-wave correlated critical Bose liquids in two dimensions, *Phys. Rev. B* **75**, 235116 (2007).
- [44] L. Yin and S. Chakravarty, Spectral anomaly and high temperature superconductors, *International Journal of Modern Physics B* **10**, 805 (1996).
- [45] T. Senthil, Critical Fermi surfaces and non-Fermi liquid metals, *Phys. Rev. B* **78**, 035103 (2008).
- [46] D. T. Son, Superconductivity by long-range color magnetic interaction in high-density quark matter, *Phys. Rev. D* **59**, 094019 (1999).
- [47] S. B. Chung, I. Mandal, S. Raghu, and S. Chakravarty, Higher angular momentum pairing from transverse gauge interactions, *Phys. Rev. B* **88**, 045127 (2013).
- [48] M. A. Metlitski, D. F. Mross, S. Sachdev, and T. Senthil, Cooper pairing in non-Fermi liquids, *Phys. Rev. B* **91**, 115111 (2015).
- [49] Z. Wang, I. Mandal, S. B. Chung, and S. Chakravarty, Pairing in half-filled Landau level, *Annals of Physics* **351**, 727 (2014).
- [50] S. Raghu, G. Torroba, and H. Wang, Metallic quantum critical points with finite BCS couplings, *Phys. Rev. B* **92**, 205104 (2015).
- [51] S. Chakravarty, R. E. Norton, and O. F. Syljuåsen, Transverse gauge interactions and the vanquished Fermi liquid, *Physical Review Letters* **74**, 1423 (1995).
- [52] A. L. Fitzpatrick, S. Kachru, J. Kaplan, and S. Raghu, Non-Fermi-liquid fixed point in a Wilsonian theory of quantum critical metals, *Phys. Rev. B* **88**, 125116 (2013).
- [53] A. L. Fitzpatrick, S. Kachru, J. Kaplan, and S. Raghu, Non-Fermi-liquid behavior of large- $N_B$  quantum critical metals, *Phys. Rev. B* **89**, 165114 (2014).
- [54] R. Mahajan, D. M. Ramirez, S. Kachru, and S. Raghu, Quantum critical metals in  $d = 3 + 1$  dimensions, *Phys. Rev. B* **88**, 115116 (2013).

- [55] G. Torroba and H. Wang, Quantum critical metals in  $4 - \epsilon$  dimensions, [Phys. Rev. B \*\*90\*\*, 165144 \(2014\)](#).
- [56] T. Senthil and R. Shankar, Fermi surfaces in general codimension and a new controlled nontrivial fixed point, [Phys. Rev. Lett. \*\*102\*\*, 046406 \(2009\)](#).
- [57] W. Kohn and J. M. Luttinger, New mechanism for superconductivity, [Phys. Rev. Lett. \*\*15\*\*, 524 \(1965\)](#).